University of South Bohemia

Faculty of Science

Deactivation of the Intramolecular Charge Transfer state in RC-LH1 complexes of genetically modified purple bacteria *Rhodobacter sphaeroides*

Master thesis

Bc. Ivana Šímová

Supervisor: Mgr. Václav Šlouf, PhD.

Consultant: Msc. Robert G. West, PhD.

České Budějovice 2019

Šímová, I., 2019: Deactivation of the Intramolecular Charge Transfer state in RC-LH1 complexes of genetically modified purple bacteria *Rhodobacter sphaeroides*. Mgr. Thesis, in English - 60 p., Faculty of Science, University of South Bohemia, České Budějovice, Czech Republic.

Annotation:

The main task of this thesis is to find the ICT activator of a carotenoid spheroidenone in the pigment-protein complex LH1 of *Rhodobacter sphaeroides*. The ICT state is characterized by a red-shifted positive transient absorption signal around 750 - 800 nm. We hypothesize that the presence of the ICT state is associated with the pigment-protein interaction of a carotenoid keto group and specific amino acid in the protein. To perform the experiment, four mutant complexes with amino acids substitutions, which should result in decreased intensity of the ICT signal due to a weaker or missing pigment-protein interaction, were obtained and measured using femtosecond time resolved pump-probe spectroscopy.

Prohlašuji, že svoji diplomovou práci jsem vypracovala samostatně pouze s použitím pramenů a literatury uvedených v seznamu citované literatury.

Prohlašuji, že v souladu s §47b zákona č. 111/1998 Sb. v platném znění souhlasím se zveřejněním své diplomové práce, a to v nezkrácené podobě elektronickou cestou ve veřejně přístupné části databáze STAG provozované Jihočeskou univerzitou v Českých Budějovicích na jejích internetových stránkách, a to se zachováním mého autorského práva k odevzdanému textu této kvalifikační práce. Souhlasím dále s tím, aby toutéž elektronickou cestou byly v souladu s uvedeným ustanovením zákona č. 111/1998 Sb. zveřejněny posudky školitele a oponentů práce i záznam o průběhu a výsledky obhajoby kvalifikační práce. Rovněž souhlasím s porovnáním textu mé kvalifikační práce s databází kvalifikačních prací Theses.cz provozovanou Národním registrem vysokoškolských kvalifikačních prací a systémem na odhalování plagiátů.

České Budějovice, 15. dubna 2019 ....

Ivana Šímová

Acknowledgements:

I would like to thank to my supervisor Václav Šlouf for reading this thesis, his constructive comments and also for inspiring discussions about the topic. I enjoyed our thesis meetings. Second thank belongs to Robert G. West for his help with the experimental part of my thesis as he taught me a lot about the whole setup used in our laboratory.

Another acknowledgements belong to all members of the Laboratory of Femtosecond Spectroscopy, namely F. Adamec, M. Durchan, M. Fuciman, T. Khan, T. Polívka and V. Šebelík for their overall contribution to the working setup. Furthermore, they all helped me with the problems that appeared during my measurements and provided me with a large amount of useful advice. E. C. Martin from the University of Sheffield, UK, is acknowledged for preparing the samples. D. Bína and F. Matoušek are both acknowledged for the HPLC analysis of measured samples. Furthermore, I would like to thank to V. Šebelík for providing me the Fig. 2.3 and also to R. Litvín for his help with data collection for Fig. 2.4.

The final thank belongs to my husband because he is the best support I could ever wish for. I am grateful to have you by my side.

List of abbreviations

AA(s) - amino acid(s)

AO(s) - atomic orbital(s)

Bchl(s) - bacteriochlorophyll(s)

Car(s) - carotenoid(s)

CC(s) - carbonyl carotenoid(s)

EADS - evolution-associated difference spectra

ESA - excited state absorption

FWHM - full width at half maximum

GSB - ground state bleaching

His - histidine

HPLC - high-performance liquid chromatography

Chl(s) - chlorophyll(s)

ICT - intramolecular charge transfer (state)

IRF - instrument response function

LH1 - light harvesting one (complex)

LH2 - light harvesting two (complex)

MO(s) - molecular orbital(s)

(N)IR - (near) infrared

OCP - orange carotenoid protein

OPA - optical parametric amplifier

Phe - phenylalanine

$Q_{x,y}$ - excited states of (bacterio)chlorophylls

RC - reaction center

$S_{0,x}$ - 0th, x-th singlet state

spn - spheroidenone

T_x - x-th triplet state

Trp - tryptophan

Tyr - tyrosine

UV-VIS - ultraviolet-visible

WLC - white light continuum, supercontinuum

YAP - yttrium aluminum perovskite

Contents

Aim of the thesis

The main task of the presented thesis is an unravelling of the intramolecular charge transfer (ICT) state activator in LH1 complex of purple bacteria *Rhodobacter sphaeroides*. Under aerobic conditions, LH1 complexes of *Rhodobacter sphaeroides* bind a carbonyl carotenoid spheroidenone [1] which, unlike other carbonyl carotenoids, exhibits a few unusual features. An incorporation of the keto group into the structure of carbonyl carotenoids results in the presence of a red-shifted positive transient absorption signal attributed to the ICT state which is usually stabilised by polar environment. [2] However, spheroidenone, the carotenoid studied in this thesis, stabilises its ICT state by protein environment. [3] This feature is attributed to the interaction between a keto group of spheroidenone and specific amino acid in the protein sequence. [3]

For the purpose of presented experiments, the primary structure of examined LH1 complexes was genetically modified to find out if substitutions of amino acids potentially interacting with spheroidenone could result in decreased intensity of the ICT signal or even its switch off.

1 Introduction

Light-harvesting complexes, including LH1, are natural molecular machines dealing with harvesting and transport of photons whose energy is then used to drive following chemical reactions. Although the main function of all light-harvesting complexes is their participation in photosynthesis that is considered as one of the most crucial biological processes, in this thesis, rather physical approach to the topic will be presented. There is one main reason for that. The primary part of photosynthesis is actually the interaction of light and matter, absorption of photons and ultrafast transfer of their energy within the molecules of whichever light-harvesting complex. What does it mean? The theoretical background of photosynthesis is largely physical and chemical, unlike the consequences which are mostly biological. Thus, to understand these actions, some knowledge of physics and chemistry is required and this is what will the first part of presented thesis be about. The second theoretical part is focused on carotenoid molecules as they play an important role within the whole photosynthetic process thanks to their wide range of applications. Moreover, all experimental parts deal with the interactions of carotenoid spheroidenone and protein environment, therefore at least a brief introduction into the behavior of carotenoids is required.

2 Molecular electronic structure

The understanding of some quantum theory principles is necessary if one wants to get the insight into the world of atoms and molecules. Despite the contemporary limits of the quantum theory, it is still a very powerful tool for the description of atoms and molecules on the microscopic level.

In classical physics, a motion of objects is expressed in terms of position $\mathbf{r}$ and momentum $\mathbf{p}$, yet this description is not applicable in a quantum mechanics. Wavefunction $\psi(\mathbf{r}, t)$, including all the information about a system, is used instead. [4] Appropriate wavefunctions are searched by solving the Schrödinger equation,

$$\hat{H}\psi = E\psi, \tag{2.1}$$

where $\hat{H}$ is defined as a Hamiltonian operator corresponding to the operator of total energy of a system and E is the energy. [5] However, the only atom which can be solved analytically without any approximation is $_1^1\text{H}$. Solutions of more complex systems are very complicated, hence some approximations have to be involved. Supposing that motions of electrons and a nucleus happen on different timescales due to their different masses, the wavefunction can be separated into two parts, nuclear and electronic. This is the so-called Born-Oppenheimer approximation which is therefore defined as

$$\psi = \mathcal{N}\mathscr{E}, \tag{2.2}$$

where $\mathcal{N}$ stands for the nuclear wavefunction and $\mathscr{E}$ is the electronic wavefunction. So, the solution can be searched for an electron with a fixed nucleus. Then, a different arrangement of a nucleus is included and following recalculations can be performed. Not only that the Born-Oppenheimer approximation simplifies the calculations of wavefunctions, the obtained solutions can also be used to establish the molecular potential energy curve (for diatomic molecules) or, generally, a surface (for polyatomic molecules). Simply put, it is the dependence of molecular potential energy on the internuclear distance. [5][6]

If the examined electronic wavefuntion contains the information about a single electron in an atom, then it is called an atomic orbital φ. However, evaluating atomic orbital wavefunctions is not an easy task and the situation becomes even more complex when it comes to molecules as it is needed to introduce the molecular orbitals. One of the most used methods is LCAO - *Linear Combinations of Atomic Orbitals.* Generally, linear combinations are characterized by a positive or negative sign whence results the existence of *bonding* (σ, π) and *antibonding* (σ^*, π^*) MOs, respectively. [6] The situation is illustrated for the molecule H_2 in Fig. 2.1. The *bonding* MO σ_s mediates the formation of a bond due to its lower energy. There are two principal types of MOs, σ/σ^* or π/π^*, depending on atomic orbitals mediating the formation of a bond. Eventually, *non-bonding* orbitals n can be introduced which refer to the lone pairs of electrons that do not participate in a chemical bond and whose energy is usually close to that of default AOs. [4]
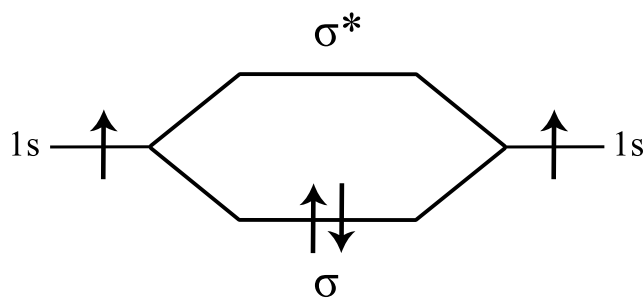

Figure 2.1: MO diagram for the formation of H_2 molecule.

Considering polyatomic molecules, MO diagrams become more branched and complicated as a lot of new MOs appear. Why is it so important to display the MO diagrams? It allows us to determine the energy levels of molecules and understand whence their whole spectroscopic activity comes from, since all molecular electronic transitions take place between different energy levels of molecules. [5]

Unfortunately, the reality is not that straightforward and it is necessary to introduce a role of the electron spin. A majority of electrons in atoms in a ground state have their spins paired. Therefore, a total spin quantum number S is 0, ground state is singlet and labeled S_0. When a photon absorption occurs, there are two possibilities. If the spin orientation of the excited electron is conserved, the resultant excited state will be singlet and labeled S_1. If not, then the spin orientation will be inverted and the excited state becomes triplet and labeled T_1. Furthermore, the energy levels contribute to a numbering of the excited states. The more energy is needed to be absorbed by a molecule to promote

4

the electron into the excited state, the higher is the number of the excited state. [6] For instance, a bonding orbital has a lower energy than a non-bonding one. It means that excited states corresponding to the mentioned orbitals will be S_2, T_2 and S_1, T_1, respectively. This electron-state diagram is illustrated in Fig. 2.2.
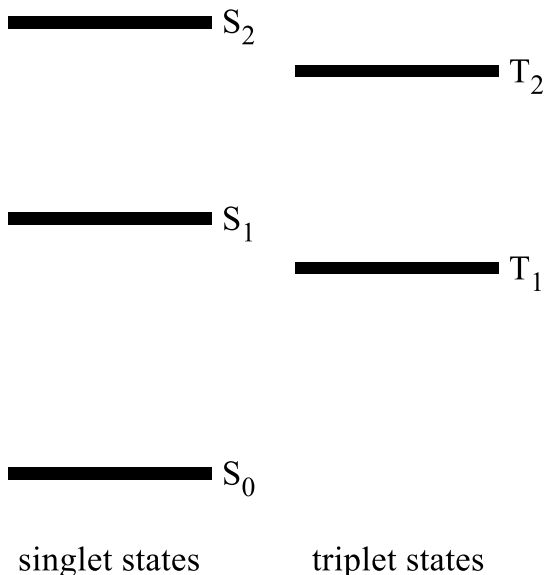

Figure 2.2: Singlet and triplet states diagram.

In Fig. 2.2, one important feature of triplet states can be recognized. In most of cases, their energies are lower than those of corresponding singlet states due to the validity of Hund's rule of maximum multiplicity. One of its consequences is that the repulsion between two electrons in different orbitals will is decreased to minimum if the electron spins are opposite. [6] It is not marked in Fig. 2.2 but it should be added that every electronic state also includes a large amount of additional vibrational and rotational energy levels. The rotational transitions will not be discussed as their energy is lower than that of vibrational transitions, therefore, their contribution to the resultant absorption spectra is significantly lower than that of electronic and vibrational transitions. The origin of vibronic (i.e. vibrational + electronic) energy levels arises from the reaction of an atomic nucleus to the change of electron distribution in the course of the electron excitation. A nucleus is exposed to a new force field and starts to vibrate. [5] The vibrational motion of a nucleus is quantized and its energy is then added to the whole energy of molecule in the form of different vibronic energy levels. [6] The vibronic energy levels of molecules can be well distinguished in their absorption spectra. [5] For example, steady-state spectra of carotenoids have typical pattern of three bands that are actually three vibrational

levels of the S_2 state. This feature is illustrated for lycopene in Fig. 2.3.
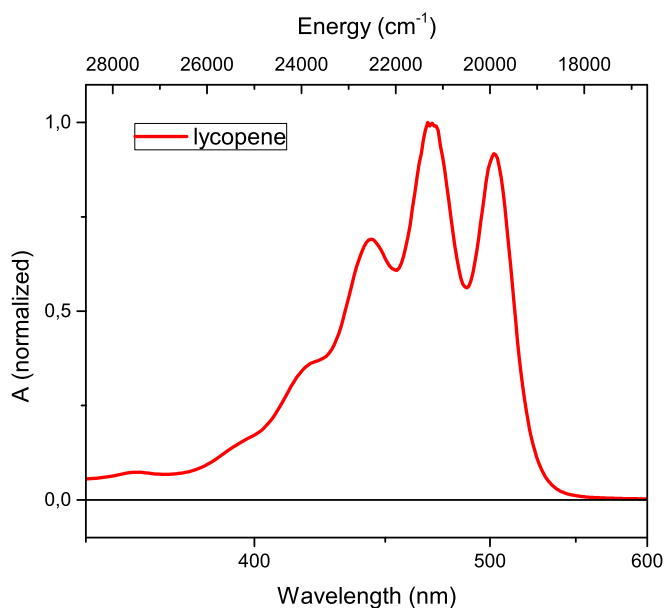

Figure 2.3: The absorption spectrum of lycopene in n-hexane.

In the end of this part, it is worth mentioning the existence of one important feature contributing to the spectroscopic activity of molecules. It is the symmetry, described by a group theory. Besides other applications, group theory is a very powerful tool for determining allowed and forbidden spectroscopic transitions. More information about symmetry and its application to the spectroscopic properties of molecules will be described in more detail in the section 3.1 which discusses the excited states of carotenoids.

2.1 Radiation and molecules

The whole field of spectroscopy is based on the interactions between photons and matter. Such interactions take place by following processes. It is a *stimulated absorption* and a *stimulated* or *spontaneous emission*. According to [7], *stimulated absorption* is a process of accepting a photon of appropriate energy $hc\tilde{\nu}$, followed by the excitation from a lower to a higher energy level.

$$M + hc\tilde{\nu} \rightarrow M^*$$ (2.3)

Spontaneous emission is a process of emitting a photon from the higher excited energy

level spontaneously, i.e. without the induction by external radiation.

$$M^* \rightarrow M + hc\tilde{\nu} \tag{2.4}$$

Stimulated emission is a process of emitting a photon from the higher energy level by the induction of external radiation.

$$M^* + hc\tilde{\nu} \rightarrow M + 2hc\tilde{\nu} \tag{2.5}$$

These phenomena were described by Albert Einstein who developed a complete theory of transition probabilites with all possible ways of photon emission being taken into account.[5] Next, the Einstein equations of changes of energy levels populations will be mentioned, according to [7]. Such equations are worth mentioning due to their relation to the transition dipole moment $\boldsymbol{\mu_{nm}}$, the important vector quantity often used in a spectroscopy. Firstly, the rate equation for stimulated absorption from a **lower energy level m** to a **higher energy level n** is given by

$$\frac{dN_n}{dt} = N_m B_{mn} \rho(\tilde{\nu}), \tag{2.6}$$

where N_n and N_m stand for the populations of n and m states, respectively, $\rho(\tilde{\nu})$ is the spectral radiation density and B_{mn} is called the Einstein coefficient of stimulated absorption. Secondly, the rate equation for stimulated emission is given by

$$\frac{dN_n}{dt} = -N_n B_{nm} \rho(\tilde{\nu}), \tag{2.7}$$

where B_{nm} is the Einstein coefficient of stimulated emission. Thirdly, the rate equation for spontaneous emission is given by

$$\frac{dN_n}{dt} = -N_n A_{nm}, \tag{2.8}$$

where A_{nm} is the Einstein coefficient of spontaneous emission.

The coefficient for stimulated emission B_{nm} can also be expressed by following equation

$$B_{nm} = \frac{8\pi^3}{(4\pi\varepsilon_0)3h^2} \mid \boldsymbol{\mu_{nm}} \mid^2 . \tag{2.9}$$

In Eq. 2.9, a probability of a transition is determined by a square of a magnitude of so-called transition dipole moment, a link between the Einstein coefficients and the wavefunctions of n and m states. The transition dipole moment is defined as

$$\boldsymbol{\mu_{nm}} = \int \psi_n^* \hat{\boldsymbol{\mu}} \psi_m \, \mathrm{d}\tau, \tag{2.10}$$

where ψ_n^* is the complex conjugate function of an excited state, ψ_m is the wavefunction of a ground state and $\hat{\boldsymbol{\mu}}$ is an electric dipole operator. The integral is calculated over all space, hence the $\mathrm{d}\tau$. [3][7] However, what is the actual origin of the transition dipole moment? It is a product of two wavefunctions and the electric dipole moment operator, integrated over all space. It is worth mentioning that the transition dipole moment does not describe following situations including the existence of electric dipoles within a molecule. Either a ground or an excited state can both have a permanent dipole moment but these dipoles are independent of time. Likewise, a transition dipole moment is not a difference between those permanent dipoles as this difference is also time-independent. The most accurate representation of a transition dipole moment is an oscillating, i.e. time-dependent electric dipole linked with the superposition state consisting of ground and excited state wavefunctions. If external radiation field appears and its oscillating frequency is same as that of a transition dipole moment in a molecule, a transition can actually happen. [8] Therefore, the possibility of transition to be allowed or forbidden depends on the value of a transition dipole moment. The allowed transitions must possess a nonzero value of $\boldsymbol{\mu_{nm}}$. [3]

Transition dipole moment $\boldsymbol{\mu_{nm}}$ is a link between the electronic structure of molecules and the possibility (and resultant intensity) of spectroscopic transitions. Origin of this fact lies in its nature as there are three main components considered to determine its final value. It is the electronic spatial wavefunction φ, the electronic spin wavefuntion $\mathcal{S}$ and the nuclear wavefuntion $\mathcal{N}$. [6]

$$\boldsymbol{\mu_{nm}} = \int \varphi_n^* \hat{\boldsymbol{\mu}} \varphi_m \, \mathrm{d}\tau \int \mathcal{S}_n^* \mathcal{S}_m \, \mathrm{d}\tau \int \mathcal{N}_n^* \mathcal{N}_m \, \mathrm{d}\tau \tag{2.11}$$

The electric dipole operator $\hat{\boldsymbol{\mu}}$ works only with the spatial wavefunctions because it depends on the electron distribution within a molecule during the excitation meaning that the terms related to the electron spin and nuclear motion can be taken out of the integral and calculated as separate overlap integrals. It is well recognizable from the Eq. 2.11 that for a transition to happen, none of the components should possess a zero value. [6] Thus, if all components have a nonzero value and incoming radiation oscillates at the appropriate frequency, there is a certain probability of the excited state formation.

2.2 Excited states

What happens after the promotion of a molecule into an excited state? This is the question to which the following chapter will attempt to answer. There are several ways of releasing the absorbed energy which can be distinguished into three main groups. There are radiative and non-radiative decays, i.e. with or without the photon emission, respectively, and quenching processes involving the energy transfer to surrounding molecules. [6] A molecule is usually excited into one of the vibrational levels relevant to the electronic excited state S_1. In the spectroscopy and related fields, a majority of studied systems are molecules in different kinds of solutions. It means that there are lots of molecules in a close distance and the vibrational energy can be transferred to the neighboring ones with the result of energy dissipation as a heat. [5] This process is called a *vibrational relaxation* and its duration is from 10^{-15} to 10^{-12} s. After the vibrational relaxation, a molecule is still in the excited state S_1 but on the 0th vibrational energy level.[9]

After the vibrational relaxation, there are three main pathways. The first one is, obviously, the opposite process to absorption and it consists in the deexcitation of a molecule from the state S_1 to the ground state S_0 accompanied by the emission of a light quantum meaning that it is a type of a radiative decay. This spontaneous emission is also known as a *fluorescence* and possesses few interesting features. Due to the validity of Franck-Condon principle, even fluorescence spectrum shows different vibrational levels of the S_0 state. In fact, the fluorescence spectrum is a red-shifted mirror image of the absorption spectrum, otherwise known as the Stokes shift. This phenomenon is caused by a small decrease of the S_1 state energy, arising from the rearrangement of surrounding molecules as a reaction to a new excited state appearance. (Fig. 2.4). [5][9]

The second pathway of deexciting a molecule into its ground state is called an *internal conversion* and it is a type of a non-radiative decay. It means that a wavefunction of an excited state overlaps with a higher vibrational wavefunction of a ground state. Then, such transition can happen and no light quantum is emitted. Of course, this process is followed by fast vibrational relaxation into the lowest energy level of a ground state S_0. [9]

For the third pathway to be introduced, a few information about the role of spin multiplicity has to be told first. A molecule is usually excited from S_0 to S_1 state, i.e.
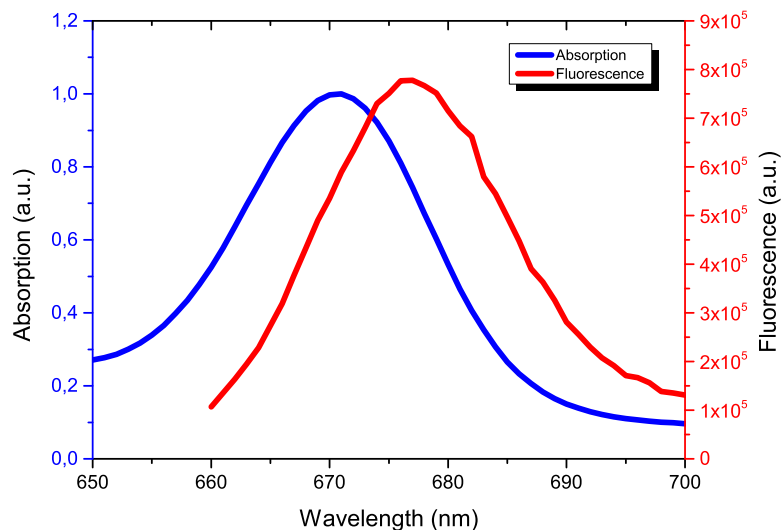
Figure 2.4: Stokes shift between the absorption and fluorescence spectrum of chlorophyll-a in pyridine.

with a spin multiplicity conserved which is in most cases followed by singlet $\rightarrow$ singlet allowed transitions back to the ground state. However, there is also a certain probability of the radiationless transition so-called *intersystem crossing* which is characterized by change of spin multiplicity. So, the singlet nature of the S_1 state is changed to the triplet one, resulting in the transformation to the T_1 state. The larger the overlap between singlet and triplet wavefunctions, the higher the probability of the $S_1 \rightsquigarrow T_1$ transition. Before the description of triplet state fates, it is worth mentioning that *singlet $\rightarrow$ triplet* transitions are considered as forbidden. However, a few mechanisms, such as spin-orbit coupling, are capable to compensate the spin change and *singlet $\rightarrow$ triplet* transitions thus become weakly allowed. The intersystem crossing takes place from the lowest energy level of an excited state S_1 to one of vibrational levels of T_1, again followed by fast vibrational relaxation. A molecule is now on the ground vibrational level of T_1 state without the possibility to return back to the S_1 as it does not possess enough energy. Thus, the only solution is to deexcite back to the ground state S_0 via the emission or the non-radiative deexcitation. Radiative decay $T_1 \rightarrow S_0$ is called a *phosphorescence*. Similarly to fluorescence, a phosphorescence is also characterized by a shifted emission spectrum to even longer wavelengths than in a case of a former process. Likewise, a shape of a phophorescence emission spectrum usually appears as a mirror image of an absorption spectrum. The second possible pathway is a non-radiative $T_1 \rightsquigarrow S_0$

deexcitation that again depends on the overlap between a wavefunction of an excited state and higher vibrational wavefunction of a ground state. However, it should be added that these processes are quite improbable as they both require a change of spin multiplity back to the singlet configuration meaning that lifetimes of triplet states are longer than those of singlet ones. [5][6][9] All the possible pathways of deexcitation mentioned above are well visualized in Jablonski diagram in Fig. 2.5.
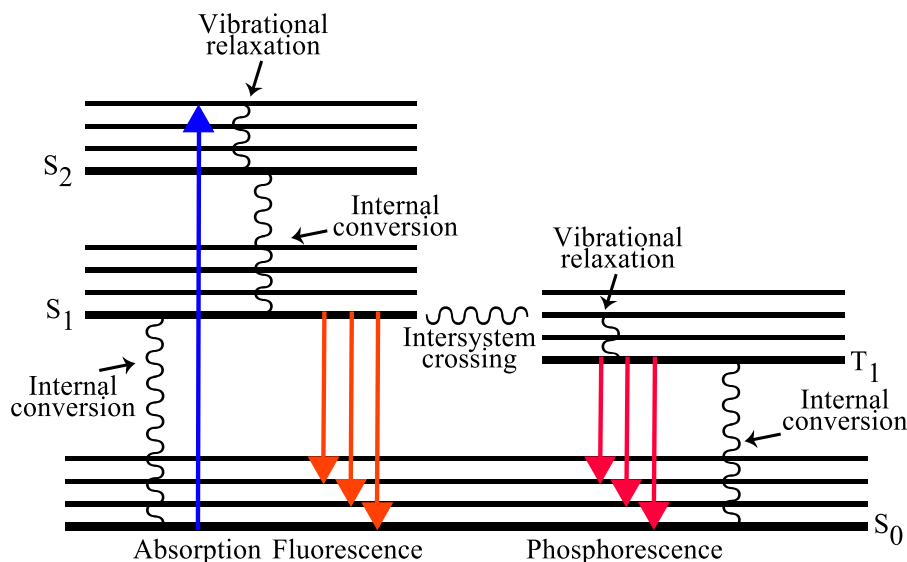

Figure 2.5: Jablonski diagram of various fates of excited states. Solid lines represent radiative transitions, wavy lines represent non-radiative ones.
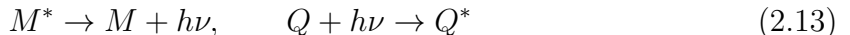
2.3 Energy transfer

Generally, light-harvesting complexes contain a large number of pigment molecules held together by structural proteins.[10] The fact that the excitation energy is transferred from one pigment molecule to another leads us to discussions about mechanisms of energy transfer between them. According to [6], the most general equation describing energy transfer is

$$M^* + Q \rightarrow M + Q^*, \tag{2.12}$$

where M^* is an excited molecule and Q is a quencher, molecule absorbing a transferred energy. The first obvious rule for a successful energy transfer is that the energy level of a quencher must be lower than (or at least the same as) that of M. If this condition is accomplished, the energy transfer will be theoretically allowed and two possible ways of performing such transfer can be introduced.

First, the energy can be transferred via *radiative process* which means that the light emitted by M^* is simultaneously reabsorbed by Q. Corresponding equations are below.

$$M^* \to M + h\nu, \qquad Q + h\nu \to Q^* \tag{2.13}$$

There are several parametres influencing the probability of radiative energy transfer between M^* and Q. However, such parametres can be summarized as follows. The larger the overlap between the emission spectrum of M^* and the absorption spectrum of Q, the higher the probability of radiative energy transfer. This probability is usually expressed in a form of the following overlap integral, according to [6],

$$P_{RT} \approx C \int_0^\infty \mathcal{F}_M(\tilde{\nu})\varepsilon_Q(\tilde{\nu})\,\mathrm{d}\tilde{\nu}, \tag{2.14}$$

where $\mathcal{F}_M(\tilde{\nu})$ is the emission spectrum function of M, $\varepsilon_Q(\tilde{\nu})$ is the absorption spectrum function of Q, both depending on a wavenumber $\tilde{\nu}$ and C is the constant depending on the concentration of Q and distance between M and Q. The value of the integral in Eq 2.14 is interpreted as the overlapping area between the emission and absorption spectrum. [6]

Secondly, energy can be also trasferred via *non-radiative processes*, i.e. without the actual emission of a photon. For a non-radiative transfer to be performed, molecules M^* and Q must be coupled by specific interactions. In most cases, two principal types of such interactions are identified, namely Coulombic and electron-exchange. Corresponding mechanisms are the Förster and the Dexter energy transfer, respectively. [3] Although the involved mechanisms are absolutely different, the probability of a non-radiative energy transfer can be generally expressed by following equation, acording to [6].

$$\frac{dP_n}{dt} = \frac{2\pi}{\hbar}V^2 \int_0^\infty \mathcal{F}_M(\tilde{\nu})\varepsilon_Q(\tilde{\nu})\,\mathrm{d}\tilde{\nu} \tag{2.15}$$

The Eq. 2.15 seems similar to the Eq. 2.14 for a radiative energy transfer as it also includes the overlap integral of $\mathcal{F}_M$ and ε_Q. Thus, the difference between those transfers lies in the origin of a V^2 term which represents the donor-acceptor coupling. [3] Coulombic energy transfer operates via a dipole-dipole intermolecular interaction of a donor and acceptor molecule. Donor molecule possesses the excited electron in the LUMO (the lowest unoccupied molecular orbital), which can be represented as an oscillating dipole. It results from the previous interaction with the radiation. This

excited electron of M^* can induce same oscillations (thanks to the static dipole-dipole interaction) of the unexcited electron in the HOMO (the highest occupied molecular orbital) of Q. These oscillations can lead to the excitation of Q electron from the HOMO to LUMO and simultaneous deexcitation of M^*. The term V^2 in the Eq. 2.15 for the Förster energy transfer can be therefore expressed by

$$V = \frac{\mu_M \mu_Q}{r^3}, \tag{2.16}$$

where μ_M and μ_Q represent the electric dipole moments of M^* and Q molecules, respectively, and r is the distance between the dipoles. Based on the mechanism described above, it can be deduced that the operating distance of the Förster energy transfer is relatively long-range (up to 100 Å). Unlike the electron-exchange energy transfer, both the excited and unexcited electron stay in a molecule and do not migrate. For the excited and unexcited electrons to be transferred between M^* and Q, molecules have to be much closer one to another, so the electron-exchange energy transfer is considered as short-range (up to 20 Å). Therefore, the most important difference between these interactions, resulting from particular mechanisms, is the range of their activity. As has been mentioned above, the essence of the electron-exchange mechanism is the replacement of the excited electron of M^* from the LUMO by the unexcited electron from Q to the HOMO and vice versa. The result is same as before, energy has been transferred from M^* to Q. [3][6] For the electron-exchange energy transfer, according to [11], the term V^2 from the Eq. 2.15 takes the following form

$$V^2 \propto e^{-2r/l}, \tag{2.17}$$

where r is the distance between M^* and Q and l represents their van der Waals radius. It can be well derived from the Eq. 2.17 that the electron-exchange mechanism works only for small distances as V^2 decreases with increasing distance of M^* and Q. Furthermore, it is worth mentioning a few information about the activity of spin multiplicity during the energy transfer as it is different for both described mechanisms. In the Förster mechanism, the electrons do not migrate from M^* to Q, so the change of spin is forbidden and only processes with a conserved spin of either a donor or an acceptor are allowed. In contrast, thanks to the actual electron exchange, a spin multiplicity does not have to be conserved in the case of the Dexter energy transfer. [3][6]

In the end of this chapter, it should be added that knowledge about energy transfer between molecules contributed to a deeper understanding of mechanisms in

the photosynthesis. [10] However, the reality is usually not that straightforward as light-harvesting complexes are very diverse systems and simple application of either Förster or Dexter mechanism is often impossible.

3 Carotenoids

Carotenoids are pigment molecules naturally occuring in a variety of organisms including bacteria, plants and even animals. [12] This wide occurrence is also apparent considering a total number of various carotenoid structures which is around 1000 so far. [13] Not only that they are present in a majority of living organisms, carotenoids also possess an abundant amount of functions. As examples, light-harvesting, photoprotective, colouring or signal functions can be mentioned. [14] For the purpose of studying photosynthesis, however, only two former functions are those we are largely interested in and will thus be discussed in following paragraphs. To understand carotenoid functions, a little information about their structure is needed to know. In terms of chemical structure, carotenoids are linear polynenes consisting of a conjugated π double bond chain binding diverse functional groups influencing the solubility and contributing to positions of absorption bands. A few examples of common carotenoid molecules are illustrated in Fig. 3.1.
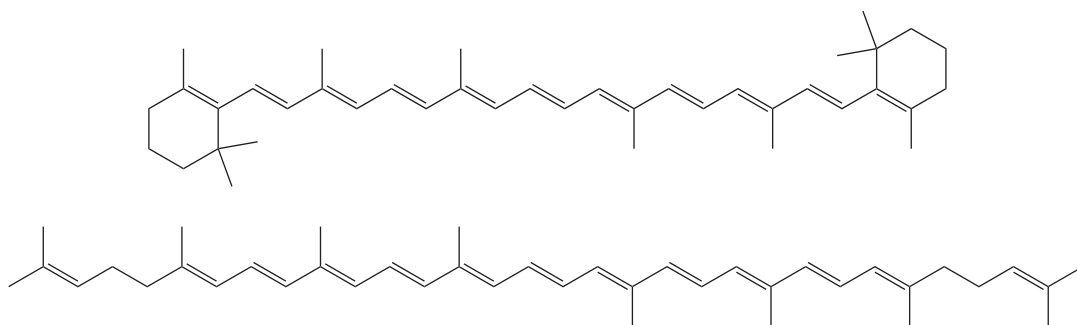
Figure 3.1: Chemical structure of β-carotene (above) and lycopene (below).

The conjugated π double bond system gives carotenoids a chromophore character. Their colours, varying from yellow to purple, are caused by a number of the conjugated bonds N (in nature, usually 7 - 13 [15]), altogether with bound functional groups. As a result, carotenoid main absorption band overlays a visible blue-green region, i.e. 400-550 nm [8], of the electromagnetic spectrum. This blue-green band explains

their involvement in a photosynthetic process because (bacterio)chlorophyll molecules possess strong absorption bands in blue (*Soret* band) and red region (Q_y band). Thus, the absorption bands of carotenoids situated in a blue-green region can increase a total number of absorbed photons and enhance the efficiency of a whole photosynthetic process. Moreover, some of carotenoid energy levels are lower than those of potentially dangerous molecules formed by high light intensities. Therefore, carotenoids are also suitable quenchers possessing important photoprotective functions.

3.1 Excited states of carotenoids

Carotenoids possess relatively atypical spectroscopic activity arising from their excited-state manifold. This statement can be demonstated by following facts. First, the strongly-allowed excited state giving carotenoids their characteristic colours is not the lowest lying excited state S_1 but the higher one, S_2, as the S_1 state is one-photon-forbidden. Secondly, the fluorescence yield is very low which is caused by fast internal conversions within a carotenoid molecule. [8]

What is the theoretical background determining the allowance or forbiddance of excited state transitions? This is the question which the following paragraph will attempt to clarify. Discussions about carotenoid photophysics are usually led towards the symmetry of linear polyene molecules. According to the group theory, molecules can be classified to various point groups based on common symmetry elements. Linear polyenes belong to the idealized C_{2h} point symmetry group meaning that corresponding symmetry operations are the identity E, the two-fold rotational axis C_2, the plane of symmetry σ_n and the centre of inversion i. [3] For every point group, it is possible to build a character table including the irreducible representations of symmetry operations. A character table generally corresponding to the C_{2h} point group is given in the Table 3.1.

C_{2h}	E	C_2	i	σ_h	translations, rotations
A_g	1	1	1	1	R_z
B_g	1	-1	1	-1	R_x, R_y
A_u	1	1	-1	-1	T_z
B_u	1	-1	-1	1	T_x, T_y

Table 3.1: Character table for the C_{2h} point group. [5]

Next, the method for determining the allowed/forbidden nature of carotenoid excited states will be presented, according to [6][16]. The symbols in the first column of Table 3.1 are labels corresponding to each row. Letters A, B serve to distinguish the symmetric (1) and antisymmetric (-1) nature, respectively, with respect to the two-fold rotational axis C_2. Similarly, subscripts g, u serve to denote the symmetry and the antisymmetry, respectively, with respect to the inversion operation i. Before the next steps will be introduced, it should be added that symmetry operations also influence the molecular orbitals. Based on the knowledge of MO shapes, it is possible to determine the impact of corresponding symmetry operations on the MO appearance. Therefore, it can be decided which rows in the Table 3.1 are valid for individual MOs and the appropriate MOs can be then labeled as A_g, B_u etc. Now, the role of previously mentioned transition dipole moment $\boldsymbol{\mu_{nm}}$ will be introduced. The Eqs. 2.10 and 2.11 show how a value of $\boldsymbol{\mu_{nm}}$ can be found. It is worth mentioning again that only the spatial wavefunction integral of the Eq. 2.11 is used as spin and nuclear wavefunctions are not directly affected by the dipole moment. Thus, the following equation is used.

$$\boldsymbol{\mu_{nm}} = \int \varphi_n^* \hat{\boldsymbol{\mu}} \varphi_m \, \mathrm{d}\tau \tag{3.1}$$

φ_n and φ_m are the electronic spatial wavefunctions of an excited and ground state, respectively. For the transition of the C_{2h} point group molecule to be allowed, the resulting transformation must be absolutelly symmetric, i.e. it must posses the A_g symmetry. Based on the procedure mentioned above, the carotenoid excited states of our interest, i.e. S_0, S_1 and S_2 are labeled A_g, A_g and B_u, respectively. The vector transition dipole moment components x, y, z transform like the translations T_x, T_y, T_z, thus, they are labeled B_u, B_u, A_u, respectively. The procedure for determining allowance/forbiddance of such transition is following. Each character of the row corresponding to the desired excited state is multiplied by the corresponding character of the row related to the transition dipole moment. Then, each character of the previous result is multiplied by the corresponding character of the row attributed to the ground state. The result is a four component symmetry expression. By comparing the result with the Table 3.1, the appropriate symmetry can be attributed to the desired transition. First, the transition $S_0 \rightarrow S_2$ will be analysed. The corresponding functions are

$$\varphi_n \mu_x \varphi_m : B_u B_u A_g = A_g, \qquad \varphi_n \mu_y \varphi_m : B_u B_u A_g = A_g, \qquad \varphi_n \mu_z \varphi_m : B_u A_u A_g = B_g.$$

Although the third expression does not have the A_g value, the $S_0 \to S_2$ is still considered as symmetry-allowed due to other expressions actually possessing it. The situation for the $S_0 \to S_1$ transition is, however, different.

$$\varphi_n \mu_x \varphi_m : A_g B_u A_g = B_u, \qquad \varphi_n \mu_y \varphi_m : A_g B_u A_g = B_u, \qquad \varphi_n \mu_z \varphi_m : A_g A_u A_g = A_u$$

From the expressions above, it is obvious that the $S_0 \to S_1$ transition is symmetry-forbidden as none of the expressions possesses the A_g value. However, it should be added that symmetry rules are strictly valid only for absolutely symmetric carotenoid molecules. [8] Furthermore, although the nature of the $S_0 \to S_1$ transition is considered as one-photon forbidden, still, it can be investigated by particular methods such as two-photon absorption spectroscopy. [17] Recently, it was pointed out that symmetry theory need not to be the only existing explanation of the $S_0 \to S_1$ transition forbiddance as it might also exist due to the coupling of a carotenoid backbone with additional functional groups wich could lead to molecular deformation of the S1 state and related one-photon inaccessibility. [18]

Next, some basic information about $S_0 \to S_2$ and $S_0 \to S_1$ transitions will be summarized. As it has already been mentioned in Chpt. 2, the $S_0 \to S_2$ transition possesses well resolved three-peak vibronic structure in the absorption spectrum. The distances between those vibronic peaks are not much affected by a number of conjugated bonds N. [19] However, both the $S_0 \to S_2$ and $S_0 \to S_1$ transition energy show the dependence on N; with increasing N, the transition energies significantly decrease. [15] Another interesting feature of carotenoid excited states is their low, yet measurable fluorescence as the preferred emission energy level is also dependent on N. Carotenoids with $N \leq 8$ fluoresce from the S_1 state. In contrast, carotenoids with $N > 8$ fluoresce from the S_2 state which is considered as the violation of so-called Kasha's rule. [20]

3.2   Carbonyl carotenoids

The previous description of excited states is valid for a majority of carotenoids. However, there exist a special group of carotenoids called carbonyl carotenoids, defining themselves by specific excited-state properties. Furthermore, carotenoid spheroidenone to which the whole experimental part of this thesis is devoted, belongs to the group of carbonyl carotenoids which justifies the following paragraphs. The structural element

defining carbonyl carotenoids is the conjugated carbonyl group which can be seen in Fig. 3.2, illustrating two typical examples of CC.
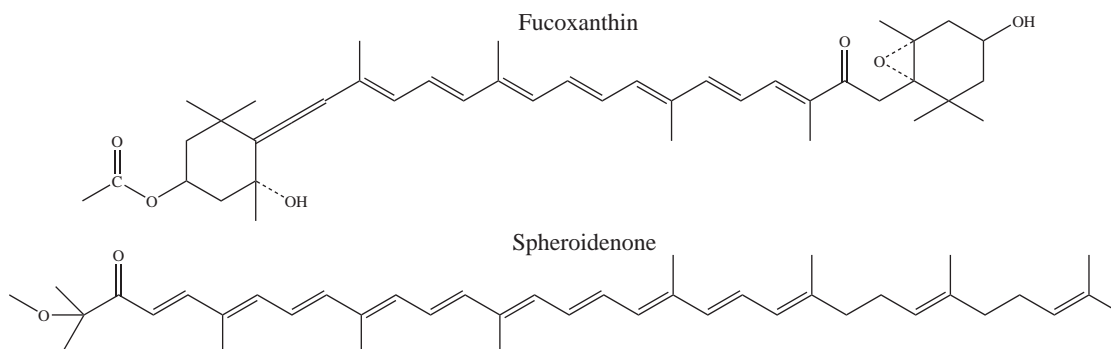

Figure 3.2: Chemical structure of fucoxathine and spheroidenone.

An incorporation of the conjugated carbonyl group into the structure of CCs results in the occurrence of so-called polarity-dependent behavior. It is characterized by a loss of characteristic three-peak vibronic structure in steady-state absorption spectra in polar solvents [15] and also by the emergence of an additional red-shifted transient absorption signal attributed to the intramolecular charge transfer (ICT) state. The intensity of the ICT state becomes larger with the increasing polarity of the solvent. [21][22] The red-shifted transient absorption signal is not the only marker of the ICT state appearance; the ICT state is also characterized by a stimulated emission in the NIR [23][24][25] and by a decrease of the S_1 lifetime. [2][21] The latter one implies the existence of a mutual interaction between the ICT and S_1 state, for instance, both sharing the same potential energy surface. [26]

It is worth mentioning that the polarity-dependent behavior does not automatically occur for all CCs. For example, the S_1 state lifetime of CC astaxanthin does not change either in a polar or nonpolar solvent [27][28] with similar results also observed for echinenone and canthaxanthin. [28][29] This feature is usually explained by the symmetric position of conjugated carbonyl groups. [29] Another CC, spheroidenone, also exhibits unusual spectroscopic properties despite its CC nature as both the ICT related transient absorption signal and corresponding S_1 lifetime shortening are not significantly different in polar and nonpolar solvents. [2] However, as has already been mentioned, spheroidenone is capable of producing a strong ICT related signal when bound in a protein. [1] The difference between spheroidenone in a solvent and spheroidenone bound in a protein may thus be in the configuration of

19

the carbonyl group with respect to the spheroidenone conjugated double bond chain. While the configuration is s-*cis* in the former case [30], in the protein it is considered as s-*trans* due to the stabilisation by protein-pigment interaction which could explain the observed strong ICT related signal. [1] Both possible configurations of the spheroidenone carbonyl group are illustrated in Fig. 3.3.
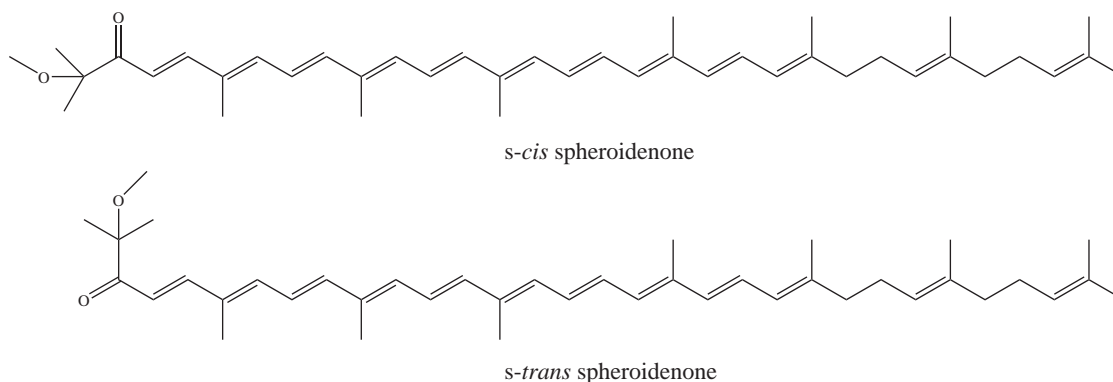

s-*cis* spheroidenone

s-*trans* spheroidenone

Figure 3.3: Chemical structure of s-*cis* and s-*trans* spheroidenone.

Observations of such strong ICT related signal of spheroidenone in the protein thus lead to discussions about possible interactions between conjugated carbonyl group and particular amino-acids. There are various possible protein-pigment interactions, yet hydrogen bonds appear quite probable due to the nature of a keto group. As search for the stabilising amino acid is the main aim of the thesis, such possible hydrogen bond interactions will be described and discussed in more detail in section 3.5.2.

3.3   Light-harvesting function of carotenoids

As has already been said, one of carotenoid tasks concerning photosynthesis is to increase the number of absorbed photons, especially in spectral regions inaccessible by (bacterio)chlorophylls. The excitation energy can be transferred via the S_2 and S_1 states to corresponding energy levels of (B)chls, pigments in which the conversion to chemical energy proceeds. (Fig. 3.4). [31]

What determines the efficiency of $Car \rightarrow (B)chl$ energy transfer? First, carotenoid excited-state lifetimes (below 300 fs for S_2 [32] and values within the ps scale for S_1 [33]) are worth considering as they are very short compared to, for instance, the (B)chl Q_y state (values within the ns scale [34]). Thus, such fast excited-state relaxations must be taken into account in the case of S_2 and S_1 mediated pathways. Next factor with
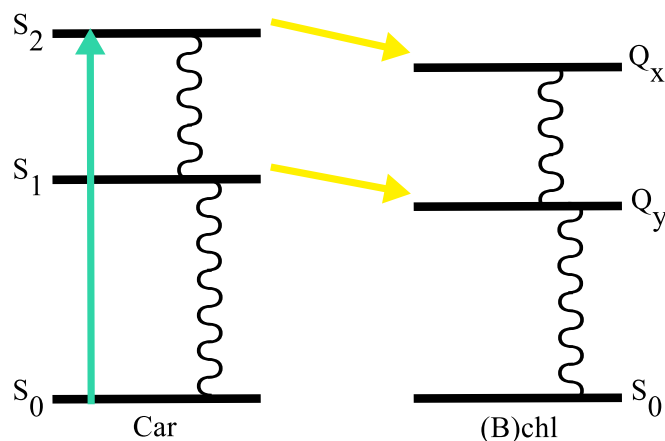
Figure 3.4: Scheme of excited states involved in $Car \rightarrow (B)chl$ energy transfer. Cyan arrow is the excitation, yellow arrows symbolise the energy transfer and wavy lines represent interval conversions.

an influence on the energy transfer is the number of conjugated double bonds N as it determines the S_1 state energies. The higher the number N, the lower the energy of the S_1 state. A majority of carotenoids in light-harvesting complexes possess N ranging from 7 to 13 which is not coincidental. For the $Car \rightarrow (B)chl$ energy transfer to be allowed, it is quite obvious that energies of carotenoid excited states must be higher than those of (B)chls. Thus, if the $N \leq 13$, the energy of S_1 state will be sufficiently high for a successful energy transfer to (B)chl Q_y state. [3][13]

Which mechanisms are involved in $Car \rightarrow (B)chl$ energy transfer? As was mentioned in the end of section 2.3, a simple application of either Förster or Dexter mechanism can be often limited because of various reasons. In the case of $Car \rightarrow (B)chl$ energy transfer, such limitations appear. They are mostly caused by the fact that interchromophore distances in light-harvesting complexes are on the order of chromophore size (approx. 20 Å) which makes the Coulombic dipole-dipole mechanism not applicable. [3] Furthermore, a forbidden nature of the $S_0 \rightarrow S_1$ transition results in a negligible transition dipole moment which also complicates or even restricts the application of dipole-dipole mechanism. [13] These discussions lead us towards the use of Dexter mechanism which is independent of transition dipole moment and operates at short distances [3] but calculations showed that its contribution to $Car \rightarrow (B)chl$ energy transfer is rather negligible. [35] Thus, satisfying results agreeing with experiments were obtained by calculating Coulombic interactions

by more advanced methods such as *transition density cube.* [36][37]

3.4 Photoprotective function of carotenoids

Light-harvesting complexes are capable of processing a certain number of incoming photons. Under such conditions, pigment molecules transfer the excitation energy to reaction centers where it is converted to chemical energy driving consequtive photosynthetic reactions. However, as the light intensity increases, these enzymatic reactions do not manage to process such energy flux. The photosynthetic machinery thus becomes saturated which can lead to unpleasant events. It is caused by the fact that the more chlorophyll molecules stay in the excited state without being quenched by photosynthesis, the higher the probability of their intersystem crossing. Unfortunately, due to long lifetimes of resultant triplet states, ^3Chl can be easily quenched by triplet ground-state oxygen which then converts to singlet oxygen $^1O_2^*$. This highly reactive molecule is known for its destructive effects on the structure of biomolecules. Therefore, photosynthetic organisms had to adapt to such situation and develop effective photoprotective mechanisms against potentially dangerous molecules. These mechanisms operate mostly via carotenoids which are able to quench several potentially dangerous excited molecules as $^1Chl^*$, $^3Chl^*$ and even $^1O_2^*$. It inevitably leads to the formation of triplet $^3Car^*$ but this superfluous energy is so low that it cannot be transferred onto another molecule in an organism, thus, it is released as heat. [3] All the possible ways of carotenoid photoprotection are schematically illustrated in Fig. 3.5.

Which mechanisms are involved in photoprotection? Considering a triplet nature of participating reactants, it can be concluded that the Förster mechanism is out of the game. Therefore, $^3Chl^*$ and $^1O_2^*$ quenching is mediated via Dexter electron-exchange mechanism as it allows *triplet-triplet* and *singlet-triplet* energy transfers. [38][39] The last one, $^1Chl^*$ quenching, is a particular sequence of reactions called non-photochemical quenching (NPQ), involving xanthophyll cycle and transmembrane proton gradient, yet the exact mechanism has not been revealed. [14][40]

Such multi-level ability of photoprotection makes carotenoids an indispensable part of light-harvesting complexes. Their presence in organisms performing the oxygenic photosynthesis is a crucial variable in the question of survival. However, it should
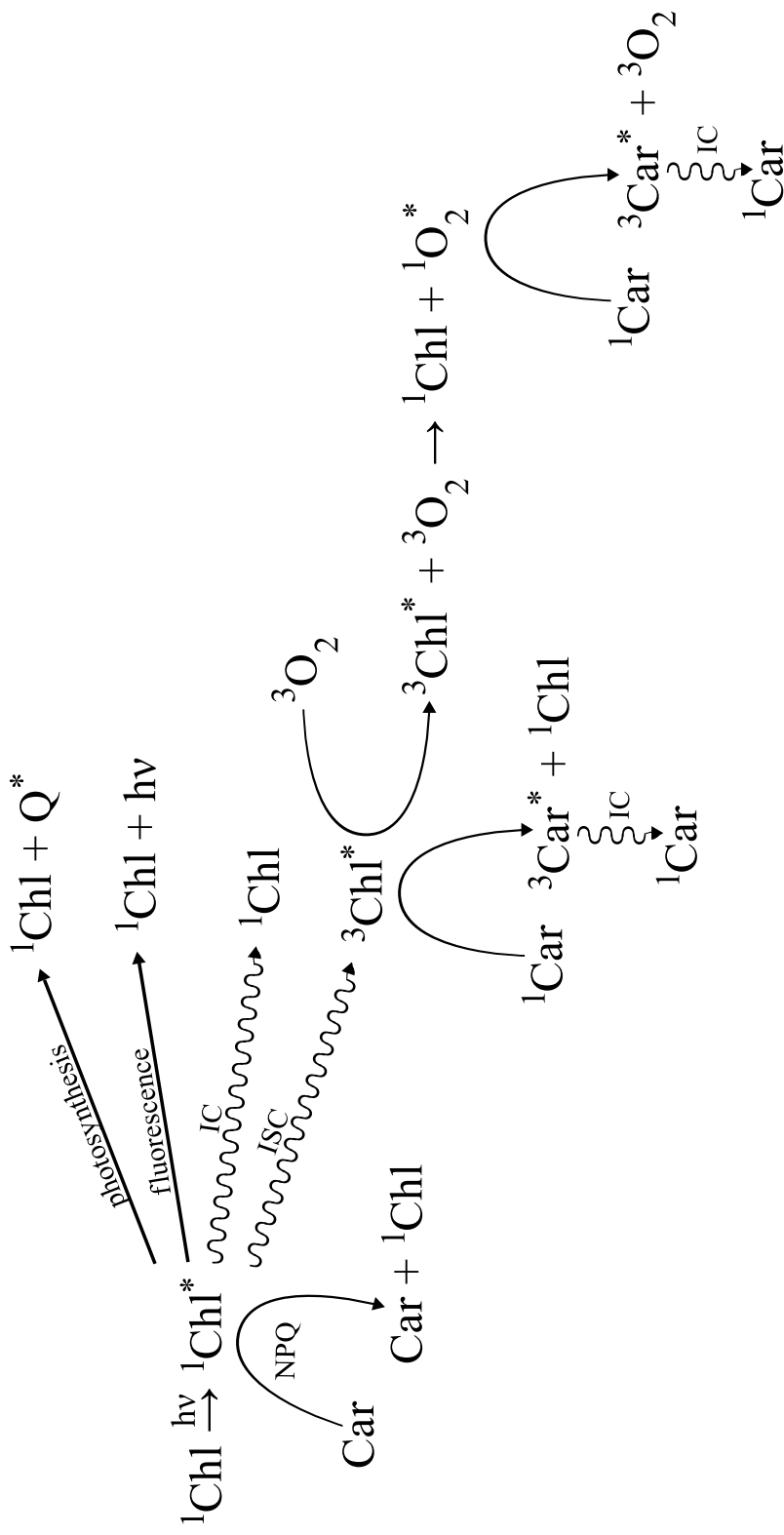
Figure 3.5: Various mechanisms of carotenoid photoprotection. In the case of NPQ, spin multiplicities of reactants are not mentioned as the exact mechanism is still unknown. Abbr.: IC - internal conversion, ICS - intersystem crossing, NPQ - non-photochemical quenching

be added that light-harvesting function is also very important especially for low-light exposed organisms as it allows them to reach sufficient efficiency of photosynthesis. [14]

3.5   Pigment protein complexes

Photosynthetic organisms had developed functional molecular structures for absorbing and processing the photon flux. Such structures are known as antenna pigment-protein complexes. As their naming prompts, antenna complexes are structures consisting of pigment molecules mediating the light-harvesting function and proteins mainly stabilising a whole complex. Depending on the type of organism and its natural habitat, antenna complexes vary both structurally and by a pigment composition. However, generally, they all share the same concept; pigment molecules transfer their excitation energy from one to another until the energy reaches its final destination, i.e. the reaction center. In the reaction center, the excitation energy is converted to the chemical one which can drive consequtive biochemical processes. Why do organisms use antennas? According to [10], about ten photons per second is absorbed by one chlorophyll molecule. Let us imagine that every chlorophyll possesses its own reaction center with the whole electron transport chain. Then, considering the chlorophyll ultrafast energy transfer, it can be concluded that the whole reaction center apparatus would be unused most of the time. This would be, of course, not economical at all. On the other hand, if the excitation energy is transferred from one chlorophyll to another, the photosynthesis will run without the interruptions caused by a photon delay.

As has been mentioned in previous paragraph, there are many varietes of antennas among the organisms based on the requirements given by their specific features and habitat. However, antennas can be also classified within the group of organisms sharing the same light-harvesting system. The most general classification of antennas is based on their contact with the lipid bilayer membrane. *Peripheral membrane antennas* are attached to the membrane from one particular side. In contrast, *integral membrane antennas* are nested in the membrane crossing its both sides. Integral membrane anntennas can be further classified into three groups pursuant to their connection with the RC which can be inseparable (*fused antennas*), separable (*core antennas*) or temporary (*accessory antennas*).

The distribution of light-harvesting pigments within antennas is visualized by the so-called funnel effect diagram (Fig. 3.6). The general idea of the funnel effect is a "downhill" energy transfer. Essentially, the longer the distance of a pigment from the reaction center, the higher energy can be absorbed by such pigment. For a successful energy transfer from a peripheral antenna complex (being quite far from the RC), the excitation energy has to pass through a lot of pigment molecules and of course, the thermal energy losses occur during the transfers. Thus, such pigment distribution ensures that the photon energy will be successfully transferred to the RC, even from more distant antennas. It is worth mentioning that funnel effect is also applicable within a single antenna complex because of carotenoids with their light-harvesting function. [10]
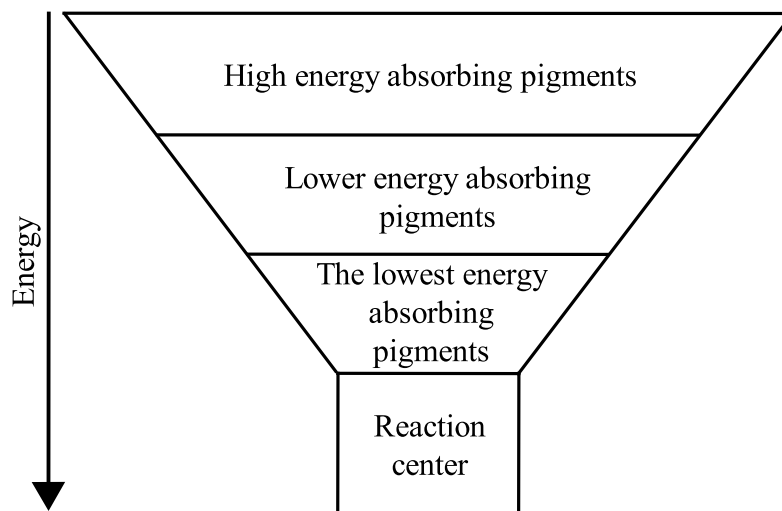

Figure 3.6: The funnel effect of energy transfer within and between antenna complexes.

3.5.1 LH2 and LH1 complex

The main task of this section is to describe main characteristics of LH2 and LH1 light-harvesting complexes. Despite the fact that the experimental part of the thesis deals with the carotenoid-protein interaction only within the LH1 complex, a few words about LH2 complex should also be mentioned to provide a brief overview on the light-harvesting apparatus of purple bacteria. A majority of purple bacteria contain LH2 and LH1 complex, together with the RC. According to the classification from section 3.5, LH2 and LH1 complexes are considered as accessory and core antennas, respectively. First, the LH2 antenna will be introduced. Based on the X-ray diffraction experiments,

it was determined that the protein structure of LH2 complex consists of an α- and β-apoprotein heterodimer subunits forming an octamer or nonamer ring. Such rings then bind carotenoid and bacteriochlorophyll pigment molecules. [41] The number of Bchls and Cars bound to one subunit was determined as 3 and 1, respectively. [42] In steady-state absorption spectra, two bands around 800 and 850 nm attributed to Bchls are observed. [43] Such spectral distinction is caused by different positions of Bchls within the heterodimer subunit; B800 Bchl is oriented perpendicularly to the heterodimer subunit, in contrast with the parallel orientation of the two B850 Bchls. Thus, B800 Bchls are relatively weakly bound unlike the B850 Bchls which are in closer contact not only with proteins but also among themselves. It enables stronger Bchl-protein and Bchl-Bchl interactions, respectively, whence results their shifted absorption band. [41]

Secondly, the structure of LH1 complex will be described. LH1 complex is a core antenna, so it encircles the reaction center. Both LH1 complex and RC form together so-called RC-LH1 complex (stoichiometrically, it is 1:1 [3]). The protein framework of LH1 is similar to LH2, LH1 also consists of $\alpha\beta$ heterodimer subunits that, in this case, form larger ring structures (approx. 16 $\alpha\beta$ subunits [10]). However, such ring structure is not the only possible spatial arrangement of LH1 complex. In *Rb. sphaeroides* and *Rb. capsulatus*, LH1 complex can form so-called S-supercomplex which is an aggregate of two LH1 complexes and two reaction centers, bound together by PufX protein and forming an S-shaped structure (Fig. 3.7). [8]

Stoichiometrically, there are two Bchls bound to one $\alpha\beta$ subunit. The Bchls in LH1 complex are analogous to B850 Bchls of LH2 [44] meaning that Bchls in LH1 are not spectrally distinguished. There is only one absorption band attributed to Bchls located around 880 nm. [8] In LH1 complex of *Rb. sphaeroides*, the maximum Bchl absorption is at 875 nm (Fig. 5.1), thus, the presented Bchls are abbreviated as B875. [44] Unlike the LH2 complex, LH1 complex can contain either one [45][46] or two carotenoids [47] bound to the $\alpha\beta$ subunit. In the case of *Rb. sphaeroides*, LH1 complexes bind two carotenoids per one $\alpha\beta$ subunit. [48]
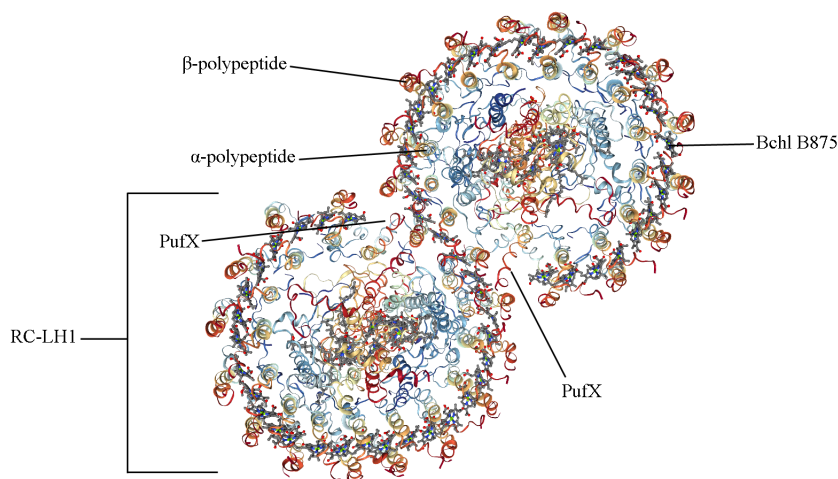
Figure 3.7: Molecular structure of RC-LH1 PufX complex with Bchls B875 and without carotenoids. Image from the RCSB PDB (rcsb.org) of PDB ID 49VG (Qian O, Papiz MZ, Jackson PJ, Brindley AA, Ng IV, Olsen JD, Dickman MJ, Bullough PA, Hunter CN) (2013) Three-Dimensional Structure of the Rhodobacter sphaeroides RC-LH1-PufX Complex: Dimerization and Quinone Channels Promoted by PufX. Biochemistry, 52:7575-7585.

3.5.2   Looking for the ICT activator in *Rb. sphaeroides*

As has already been mentioned, this thesis aims to perform transient absorption experiments on LH1 mutant samples possessing various AA substitutions. Thus, the task of this section is to present the measured samples. All mutants are of the RC-LH1 PufX shape (Fig. 3.7) with the carotenoid spheroidenone. The story about the spheroidenone ICT state appearance is presented above in section 3.2, so a quick walkthrough will follow. According to [1], we hypothesize that the s-*trans* configuration of spn, considered as crucial for the ICT state activation, is stabilised by a protein environment due to the pigment-protein interactions, supposedly by a hydrogen bond. The set of measured LH1 mutants lacks various putative hydrogen bond pigment-protein interactions because of AA mutations. Before they will be discussed, the sequences of B875 α and β LH1 polypeptides will be introduced in Fig. 3.8.

The reasons for searching the possible ICT activator in such protein region, i.e. near the N-terminus, will be clarified, according to [3]. It seems logical that a polar keto group of spn would interact with a polar part of the protein which is N- or C-terminus. Furthermore, according to [41][49], the polar part of spheroidenone is
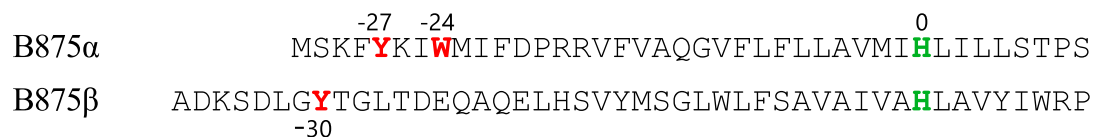
```
                         -27   -24                                    0
B875α            MSKFYKIWMIFDPRRVFVAQGVFLFLLAVMIHLILLSTPS

B875β     ADKSDLGYTGLTDEQAQELHSVYMSGLWLFSAVAIVAHLAVYIWRP
                    -30
```

Figure 3.8: Sequences of B875 α and β LH1 polypeptides. Green His is conserved in various LH1 α and β polypeptides, therefore labeled as 0. Red AAs are potential ICT state activators. The numbering is given with respect to the 0 His. N-terminus of the polypeptides is on the left.

oriented at the N-terminus. Thus, AAs suspected of the ICT state activation will be searched near the N-terminal part of either α or β polypeptide. The approach used to find possible ICT state activators was based on the analogy with the Orange Carotenoid Protein (OCP) binding the carotenoid 3-hydroxyechinenone. A CC echinenone has the same feature as spheroidenone; it does not exhibit the ICT signal in solution [29], on the other hand, the ICT signal is observed when echinenone is bound in OCP. [50] According to [50], a configuration of 3-hydroxyechinenone in OCP is close to the s-*trans*. Moreover, AAs nearest to its keto group were identified as Tyr and Trp, both capable of hydrogen bond interaction (see Fig. 3.9). [51]
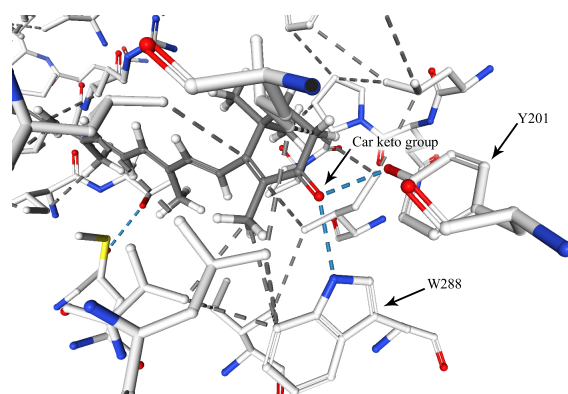

Figure 3.9: Hydrogen bond interactions between a keto group of 3-hydroxyechinenone and neighboring AAs Tyr201 and Trp288. [52] There are no significant differences between the positions of echinenone and 3-hydroxyechinenone in OCP. [51] Blue dashed lines represent hydrogen bonds. Image from the RCSB PDB (rcsb.org) of PDB ID 5TV0 (Bandara S, Ren Z, Lu L, Zeng X, Shin H, Zhao KH, Yang X) (2017) Photoactivation mechanism of a carotenoid-based photoreceptor. Proc Natl Acad Sci USA, 114:6286-6291.

Thus, it is assumed that Tyr and Trp near the N-terminus of LH1 complex could also stabilise the s-*trans* configuration of spn. Such three possible AAs were found in the sequences and they are highlighted in Fig. 3.8. It is αTyr-27, αTrp-24 and βTyr-30. For the purpose of presented experiments, αTyr-27, αTrp-24 and βTyr-30 were all substituted by phenylalanine Phe, incapable of hydrogen bond interaction.

4 Materials and methods

4.1 Sample preparation

In the beginning, it should be mentioned that sample preparation was not the objective of this thesis and the author of the thesis participated neither at the genetic modification nor at the isolation of the samples, so only concise information about genetic modification and isolation of measured mutated LH1 complexes will be presented.

The method of genetic modification will be described in following paragraphs, according to [53]. The modified $\Delta puc1BA\Delta puc2BA\Delta pufBA$ strains were obtained by series of deletions and reinsertions of $puc1BA$, $puc2BA$, genes responsible for coding LH2 [54], and $pufBA$, gene coding LH1. [55] DNA regions $\sim$400 bp upstream and downstream of the appropriate genes were amplified using PCR. PCR primers were designed in such a way that final fragments of genomic sequence lacked the $puc1BA$, $puc2BA$ and $pufBA$ genes. These fragments with omitted genes were incorporated into $Rb.$ $sphaeroides$ by ligation of fragments to the pK18mobsacB vector which was then transferred into the cells. Successful transfer was confirmed by PCR sreening. The deletions of genes resulted in a reduction of a PCR product size and mutations were then confirmed by DNA sequencing. The X1 mutant was completely generated during the procedure descibed above as it was not needed to incorporate any amino acid substitution into its $pufBA$ gene unlike the rest of mutants (BX4, BU1, BY23). Next, the $pufBA$ genes with appropriate mutations were generated by overlap extension PCR. The final PCR products with amino acid substitutions were ligated to the pK18mobsacB vector which was then used to insert the mutated $pufBA$ gene into the $\Delta puc1BA\Delta puc2BA\Delta pufBA$ $Rb.$ $sphaeroides$ strains. Successful integration of mutated $pufBA$ gene was then confirmed by an increase of a PCR product size, followed by DNA sequencing. The obtained mutants are specified in the Table 4.1 below.

Mutant	Gene modification	AA substitution
X1	$\Delta puc1BA\Delta puc2BA$	N/A
BX4	$\Delta puc1BA\Delta puc2BA\Delta pufBA$	αY-27F
BU1	$\Delta puc1BA\Delta puc2BA\Delta pufBA$	βY-30F
BY23	$\Delta puc1BA\Delta puc2BA\Delta pufBA$	αW-24F

Table 4.1: Specification of the modified measured LH1 complexes. X1 is the test sample meaning that it does not contain any AA substitution. The numbering of all mutants is related to the absolutely conserved Histidine labeled as 0. Abbr. Y - Tyrosine, W - Tryptophan, F - Phenylalanine

The method of RC-LH1 complexes isolation will be described here, according to [56]. Modified strains were grown semi-aerobically. Grown cells were harvested by a centrifugation, lysed in a French press and centrifuged again. Internal membranes were applied to the sucrose gradient and centrifuged. The next steps were harvesting, solubilising in 20 mM HEPES, pH 7.5, 1 mM EDTA containing 4% w/v β-DDM at 4 °C for 1 hour, while stirring in the dark and then centrifuged again. Solubilised proteins were applied to the sucrose step gradients in 20 mM HEPES, pH 7.5, 1 mM EDTA containing 0.04% w/v β-DDM comprising five steps with increments of 1.25% sucrose concentration in ultracentrifuge tubes and centrifuged. Complexes from the sucrose gradient were bound to a 25 ml DEAE Sepharose column pre-equilibrated with five column volumes of 20 mM HEPES, pH 7.5, 1 mM EDTA containing 0.04% w/v β-DDM. The column was washed fivefold with a buffer. Complexes were eluted in 20 mM HEPES, pH 7.5, 1 mM EDTA, 0.04% w/v β-DDM. Fractions corresponding to the highest purity were diluted twofold in column buffer, pooled and reapplied to the DEAE column. After two rounds of ion-exchange chromatography, the size exclusion chromatography was performed to purify the samples. Fractions with the highest purity were pooled, concentrated and aliquoted. All the samples were stored at -80 °C.

Prior to performed time-resolved experiments, all samples were dissolved in a 20 mM HEPES, pH 7.5, 1 mM EDTA and their absorbance at the excitation wavelength, i.e. 555 nm, was adjusted to 0.35 OD, measured in a 2-mm quartz rectangular cuvette.

Steady-state absorption measurements were all performed on Agilent 8453 UV–VIS spectrophotometer.

4.2 Spectroscopy

Spectroscopy is probably one of the most used experimental methods, mainly due to its large variability. Based on the interaction between the electromagnetic radiation and matter, it allows us to study behavior of various systems (e.g. solutions, crystals, etc.) on different levels. Generally, electromagnetic radiation is divided into several groups according to the frequencies. Every such group possesses a different effect on the atomic or molecular structure, therefore, it is possible to obtain information about molecular vibrations, electronic transitions, etc. With regard to processes we mainly deal with, i.e. electronic excited states of chromophore molecules, our region of interest is thus the UV-VIS(NIR). Another point of view is a type of interaction between radiation and matter whence result techniques such as absorption, emission as well as Raman spectroscopy. The general output of spectroscopy methods is a spectrum, including particular information about a measured system depending on the used method. Even steady-state spectroscopy techniques provide a large insight into measured samples and related processes, yet the outputs of such methods do not contain any information about the dynamics of observed processes. To obtain such a kind of information, time-resolved techniques must be employed.

4.2.1 Time resolved pump-probe spectroscopy

As has been mentioned in Chpts. 2, 3, a majority of photosynthetic processess connected to energy transfer via pigment molecules take place on an ultrafast time scale, i.e. from hundredths to hundreds of ps. With the development of ultrashort laser pulses (∼100 fs) and their detection, suddenly, a dynamics of femtosecond or picosecond processes could have been studied in real-time which significantly contributed to more profound knowlegde in the field of photosythesis. [57] One of the basic time-resolved techniques using the ultrashort pulses is called a transient absorption pump-probe spectroscopy. The insight into the behavior of excited states is achived by the excitation of a sample with *pump* pulse, being followed by *probe* pulse which is delayed with respect to the pump pulse and whose intensity is then detected.

The time delay of probe with respect to pump is adjustable, meaning that a change of absorption is recorded again at longer times. Therefore, the information about excited state dynamics is obtained.

However, to achieve a working pump-probe setup, a lot of different aspects must be taken into account. Therefore, the most important ones will be outlined in this paragraph. The cornerstone of pump-probe experiments is the laser system providing ultrashort pulses, usually with a wavelength ∼800 nm. To separate pump and probe, the main beam is split into two. As totally opposite features are required for pump and probe pulse, each of them then follows a different pathway. The pump pulse promotes molecules into an excited state, so it should be tuneable (as a good example, let us consider Chl and Car, both absorbing different wavelengths) and spectrally narrow (to reach the so-called spectral selectivity, i.e. to excite only desired molecules). Such requirements are achieved in the *optical parametric amplifier* (OPA). Not only that this device is able to generate various wavelengths thanks to various nonlinear processes, it also amplifies the final signal by the process of parametric amplification. In contrast, the probe pulse should be spectrally broad to span regions with expected transient absorption signals. To achieve such broad spectrum, a supercontinuum generation in various crystal plates is mainly used. Moreover, one of the pulses has to pass through the delay device to achieve the desired time delay between pump and probe. Thus, the adjustable delay line is placed into its pathway. The pathways of pump and probe pulses then cross in the sample. After the sample perturbation, pump pulses are blocked and probe pulses are aimed into the detector. The simplified scheme of the pump-probe experiment is illustrated in Fig. 4.1.

4.2.1.1 Experimental setup

All the time resolved experiments in this thesis were performed with the experimental setup described in this section, according to [58] and illustrated in Fig. 4.2. The laser system generating femtosecond pulses is based on the Ti:sapphire regenerative amplifier (Spitfire Ace-100F, Spectra-Physics) consisting of Ti:sapphire oscillator (MaiTai SP, Spectra-Physics) and pumped by Nd:YLF laser (Empower 30, Spectra-Physics). Resultant ultrafast pulses possess following parameters: central wavelength ∼800 nm, pulse duration ∼110 fs, repetition rate 1 kHz. The main output is then divided into pump and probe beam by a beam-splitter. The wavelength of
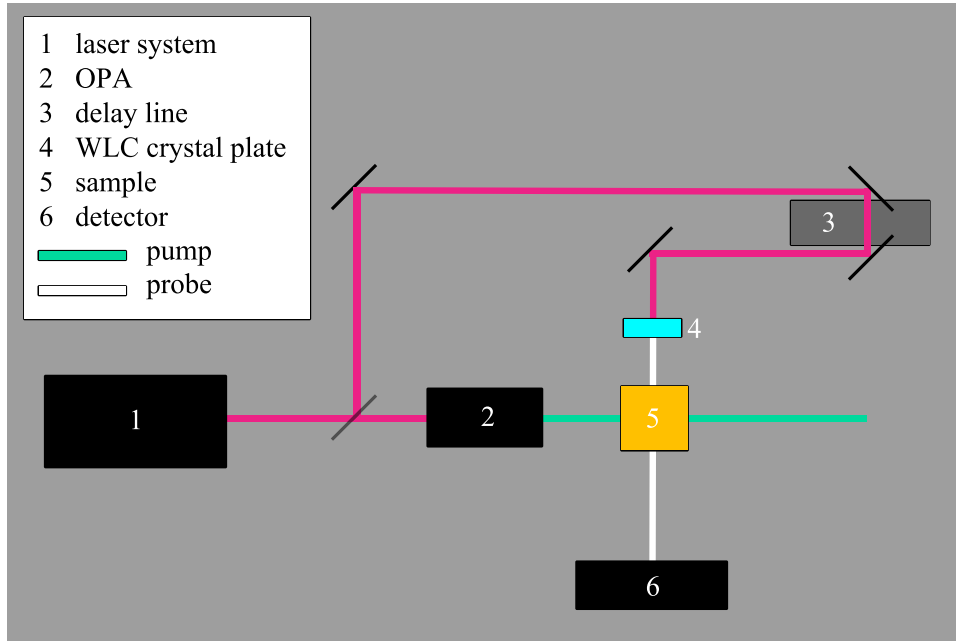
Figure 4.1: Simplified scheme of the pump-probe experiment.

pump pulses is tuned by the OPA (TOPAS Prime, Light Conversion). Next, a chopper
is placed into the pathway of pump beam to block every second pulse which serves to
increase a signal/noise ratio (see Eq. 4.1). Pump beam is then focused into the sample,
being blocked afterwards. The pathway of probe beam is first led to the OPA to
generate ~1300 nm pulses, then the probe pulses pass through the delay line to achieve
a desired time difference. Next, the WLC is generated by passing a probe beam
through a crystal plate (in this thesis, two different crystal plates were used for NIR
and VIS experiments, so see below for exact characteristics). Resultant WLC probe
beam is collimated with a parabolic mirror and divided into the probe and reference
beam by a beam-splitter. Then, both beams are focused at in the sample. While
the probe beam passes through the same spot as pump beam, the reference beam
passes nearby. After perturbing the sample, both the probe and reference beam are
focused into the entrance slit of a spectrometer in which they are dispersed by
a grating onto a double CCD array.

For all experiments presented in this thesis, the excitation wavelength was set to
555 nm and the power of pump pulses was maintained around 200 µW. The mutual
polarization between pump and probe beam was set to the so-called *magic angle*, i.e.
54.7°, to avoid anisotropy effects. The main difference between NIR and VIS experiments
was in the way of supercontinuum generation. For the NIR region, ~1300 nm pulses were
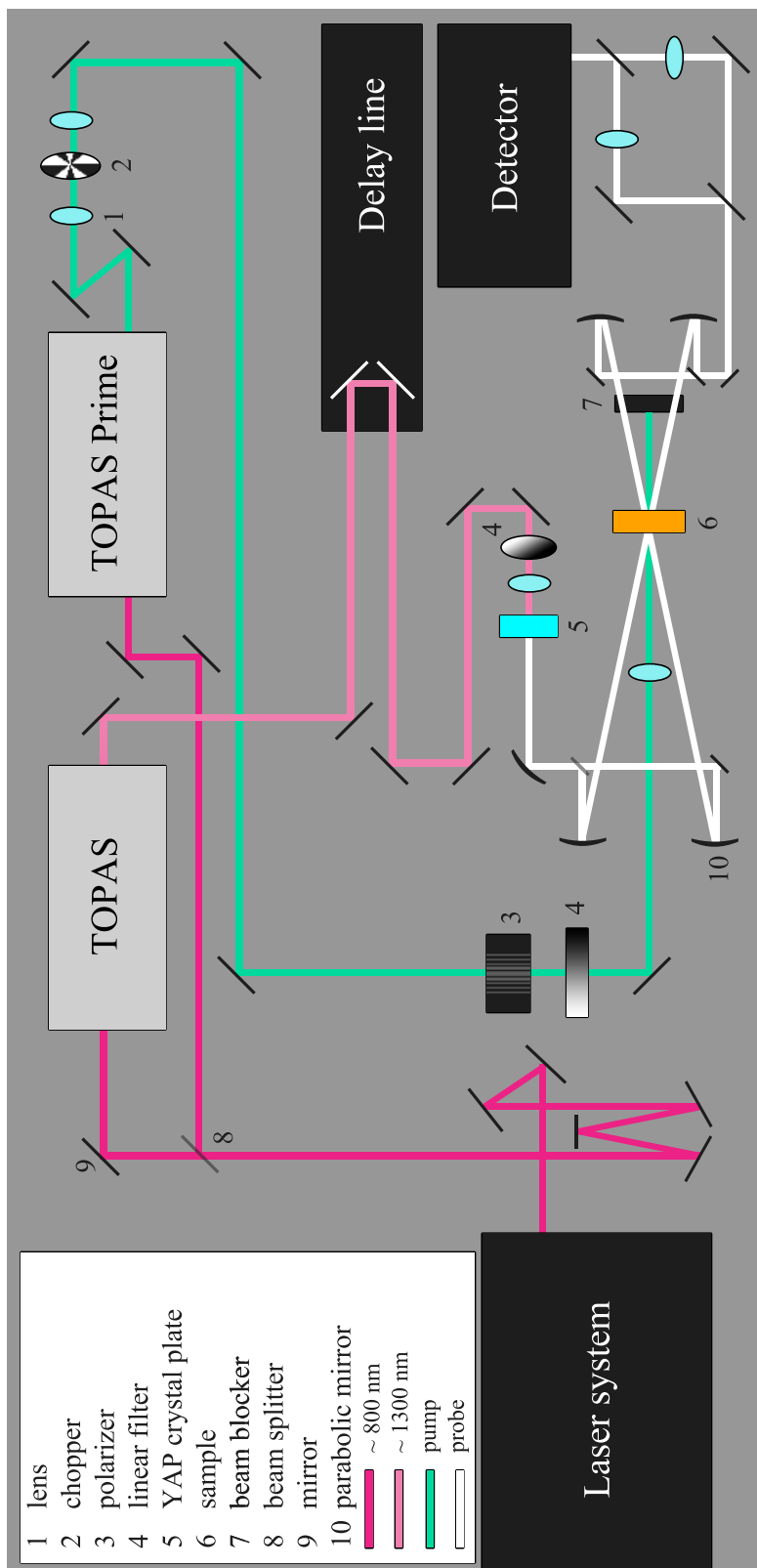
Figure 4.2: Experimental setup of pump-probe spectroscopy that was used for the measurements in NIR region.

generated by a store-bought OPA (TOPAS, Light Conversion) and WLC was generated by 2.95 mm YAP crystal plate. Spectral window of NIR measurements was set to 800 – 1100 nm. In contrast, for the VIS region, ~1300 nm pulses were generated by a home-built OPA and WLC was generated by 3 mm CaF_2 crystal plate. Spectral window of VIS measurements was set to 500 – 780 nm. During the experiment, each sample was stirred with a magnetic stirrer placed inside a cuvette to prevent its degradation. All measurements were performed at room temperature.

4.2.1.2 Transient absorption signals

From the description of experimental setup in section 4.2.1.1, it can be deduced that three different values of beam intensities arrive to the detector. It is the intensity of pre-pumped probe I_{pp}, the intensity of unpumped probe I_{up} and the intensity of reference beam I_{ref}. Total change of absorption is then calculated by using the following equation. [3]

$$\Delta A(\lambda, \Delta t) = \log \frac{I_{ref}}{I_{pp}} - \log \frac{I_{ref}}{I_{up}} \tag{4.1}$$

In general, three contributions to the overall transient absorption signal are distinguished. [57]

Ground state bleaching: The first contribution to the transient absorption signal results from a low concentration of molecules in their ground state after the sample is excited. Thus, as the probe beam passes through the pre-excited spot, fewer photons are absorbed in a ground state absorption region than for the reference beam passing through the non-excited spot. Consequently, $I_{pp} > I_{ref}$ and the change of absorption will be negative.

Stimulated emission: As mentioned in section 2.1, the deexcitation of a molecule can be induced by a radiation passing through. The probe beam interacts with the pre-excited sample, hence its photons can cause such process. Emitted photon possesses absolutely same parametres as the stimulating photon, therefore, it also arrives to the spectrometer which then detects more photons for I_{pp} than for I_{ref}, whence results the negative signal.

Excited state absorption: The third contribution to the overall transient absorption signal arises from the existence of optically allowed transitions between the excited states. Thus, molecules excited by pump beam can absorb photons of probe beam which are specific to their allowed transition to even higher excited states. As a result, less photons of probe beam arrive to the detector, hence $I_{pp} < I_{ref}$ and resultant ΔA will be positive.

Although the contributions mentioned above are the most frequent, they are not the only ones. The excitation can cause a formation of additional states, e.g. triplet states absorbing in specific regions, resulting in the occurrence of a positive signal. This is called a *product absorption*. The last mentioned possible contribution to the transient absorption signal can be well demonstrated on photosynthetic complexes. Upon excitation of carotenoid molecules, the energy transfer between Car(s) and Bchl(s) takes place, followed by occurrence of Bchl GSB signal in NIR region. Therefore, Bchl(s) contribute to the overall transient absorption signal, even if they have not been directly excited.

4.2.2 Data analysis

All measured pump-probe data were analysed by global fitting method in the program DAFit (Pascher Instruments). To use a global fitting analysis, a few data correction procedures must precede. First, the chirp correction is applied to a whole measured dataset. Secondly, the instrument response function is deconvoluted. Thirdly, a global fitting model (in this case, the sequential one) can be finally applied, whence results a set of so-called EADS (evolution-associated difference spectra). Why do data have to undergo such procedures? Simply said, the first interactions between pump and probe take place in the blue region of the probe meaning that signals in the blue region are detected earlier than those in the red region. This phenomenon is called the chirp. The task of chirp correction is thus assigning the same zero time within the measured spectral range. As a result, events in the blue and red region now appear at appropriate times with respect to the zero. The IRF is a convolution of the excitation pump pulse and the probe pulse. For the analysis of pump-probe experiments, the IRF is usually fitted as a Gaussian function with FWHM ~120 fs. [57][59]

After the procedures mentioned above, the sequential model can be applied on the corrected dataset. The sequential model consists of a set of gradually evolving compartments representing the spectral evolution of the whole system, i.e. *evolution-associated difference spectra* EADS. EADS can be expressed as

$$A \xrightarrow{\tau_1} B \xrightarrow{\tau_2} C \xrightarrow{\tau_3} D \xrightarrow{\tau_4} E...,$$
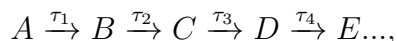
where A, B, C, etc. are the individual compartments and τ_x are their corresponding lifetimes. EADS are interpreted as follows. The compartment A decays with the first

37

lifetime τ_1, whereas, simultaneously, the second compartment B appears. Similarly, the second compartment B decays with the second lifetime τ_2 and at the same time, the third compartment C appears. As an ideal example, individual compartments should represent corresponding excited states. The existence of some mismatches can indicate, for instance, that the studied system decays into two different states. To get an insight into the evolution of such processes, a target analysis can be used. [3] However, for all measurements presented in this thesis, a global analysis was sufficient.

5 Results

5.1 Steady-state spectra

The steady-state absorption spectra of all measured samples were taken before time-resolved experiments and they are shown in Fig. 5.1.
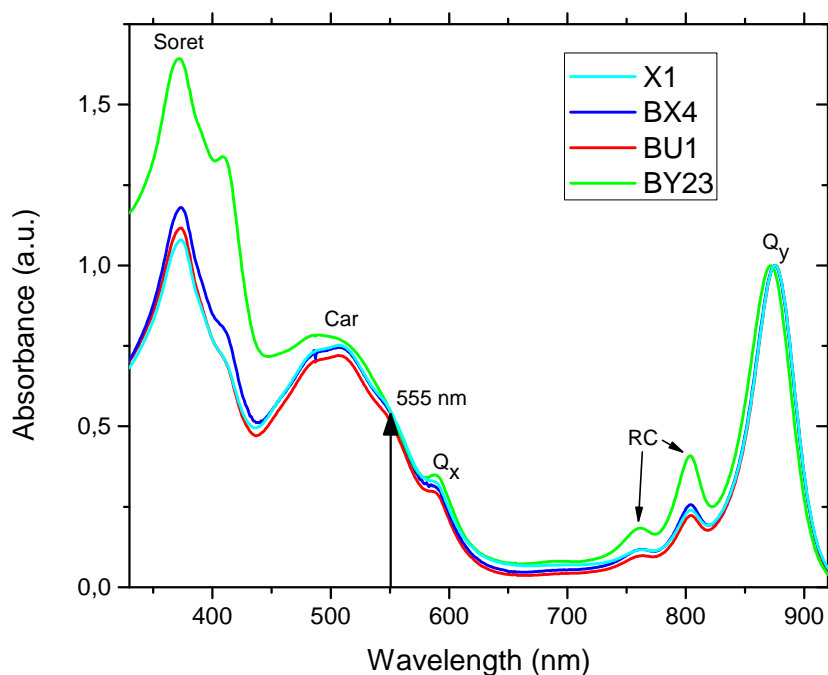

Figure 5.1: Absorption spectra of RC-LH1 PufX spn mutants, normalized to the maximum of Q_y. Soret, $Q_{x,y}$ - bacteriochlorophyll-a absorption bands, RC - pigments of reaction center, Car - spheroidenone absorption band, arrow - excitation wavelength

In Fig. 5.1, a typical pattern of RC-LH1 complexe can be recognized. The blue region is dominated by Bchl Soret band peaking at $\sim$373 nm, similarly to the red region with Bchl Q_y band peaking at $\sim$875 nm. Another Bchl band, Q_x, can be found at $\sim$590 nm. Two weaker absorption bands in the red region correspond to the pigments of RC, Bchls

and bacteriopheophytins, with their maxima at ∼804 nm and ∼760 nm, respectively. In the blue-green region, characteristic absorption band of spheroidenone is observed; however, its vibronic structure is lost and exact values of 0-0, 0-1 and 0-2 transitions are difficult to be identified. The lost of vibronic structure is likely caused by a presence of two spheroidenones possessing slightly different configurations of their carbonyl groups or by a conjugated carbonyl group itself, interacting with the environment outside the protein. By taking a closer look on the differences between particular mutants, it can be concluded that the absorption spectra of all mutants are more or less the same with one exception, which is BY23. Not only that this mutant has Bchl Q_y maximum shifted to 872 nm, but also its whole absorption spectrum is affected by a scattering. The excitation wavelength was set to 555 nm, i.e. the probable, yet weakly distinguished position of carotenoid 0-0 ($S_0 \rightarrow$ 0th vibrational level of S_2 state) transition.

5.2   Transient absorption spectra

To search for the ICT state deactivation, all samples were excited by 555 nm. Due to AA substitutions and potential disruption of spn s-*trans* configuration, changes of the ICT state intesity were expected. Thus, we focused on transient absorption spectra at the time when the maximal intensity ot the ICT state was recorded which is 0.15 ps for all measured samples. Transient absorption spectra at 0.15 ps were then compared and this comparison is shown in Fig. 5.2. As the excitation wavelength was aimed on spheroidenone 0-0 transition, all presented spectra in Fig. 5.2 report a typical pattern of excited carotenoid in RC-LH1 PufX spn complexe; the Car GSB in the blue-green region, the $S_1 - S_N$ transition signal peaking at ∼600 nm and the profound ICT signal with its maximum at ∼742 nm. [1] It can be immediately recognized that the intensity of the ICT state of the BY23 mutant is lower compared to the other samples. On the other hand, no significant change of the ICT state intensity is observed for the BX4 and BU1 mutants, both being indistinguishable from the sample X1 without any AA substitution. Thus, the AA substitution in BY23 might be considered as the first hint in the looking for origin of the ICT state activation.

Next, the results of the global fitting analysis of the data in VIS region will be presented in the form of EADS which can provide deeper insight into the carotenoid excited-state dynamics. A collection of EADS for all measured mutants is shown in
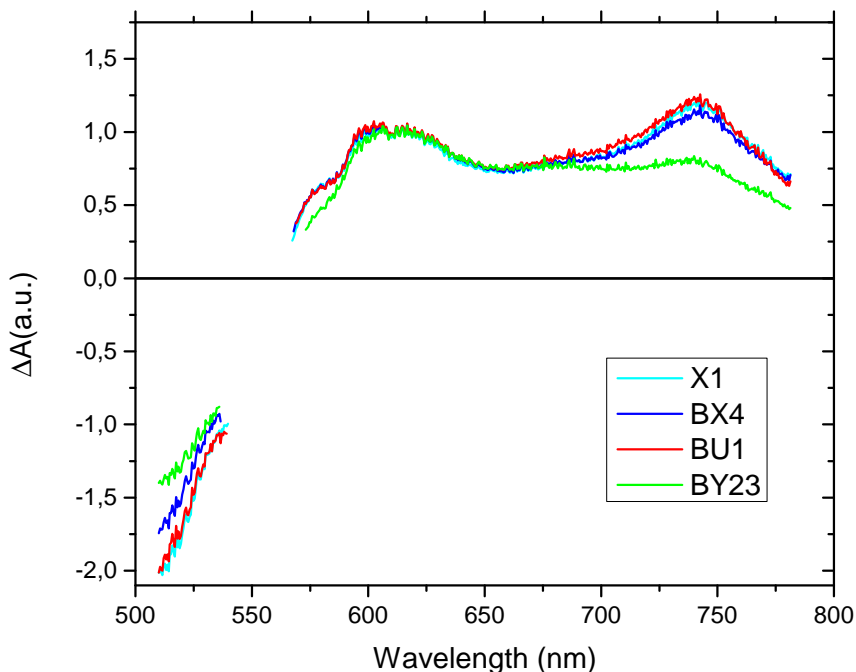
Figure 5.2: Transient absorption spectra of all measured mutants after 555 nm excitation, taken at 0.15 ps and normalized at ∼615 nm.

Fig. 5.3. By taking a look at the EADS corresponding to particular mutants, it can be noticed that they all possess very similar features. Thus, the detailed explanation of excited-state processes will be given only for the X1 mutant, i.e. the one without any AA substitution, as it is supposed to represent a typical behavior of RC-LH1 PufX spn complex. Generally, first EADS are often not realistic because of the similarity of its time constant and the pulse duration. We will thus avoid any definite attributions to physical processes in the sample; however, it should correspond to the decay of the Car S_2 state at <0.1 ps. Simultaneously, the second EADS (green) appears, clearly representing both the Car S_1 and ICT state due to the presence of S_1 and ICT related signals at ∼600 nm and ∼750 nm, respectively. Moreover, weak yet distinguishable Bchl Q_x bleaching is observed at ∼590 nm. The second EADS decays in 0.6 ps and at the same time, the third one (yellow) appears. The yellow EADS contains a weaker Car S_1 signal and profound dip at the region of Bchl Q_x bleaching, so the excited states corresponding to the second EADS serve as the main energy donors for Bchls. [1] The events corresponding to the third EADS are however quite ambiguous, hence will be discussed in following chapter. This EADS decays in 3.2 ps and gives rise to the fourth EADS (orange), in
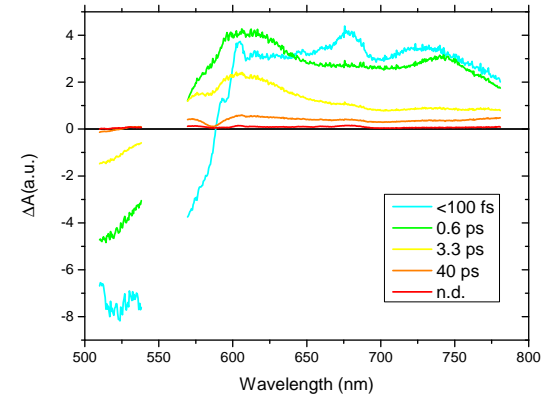
(a) X1
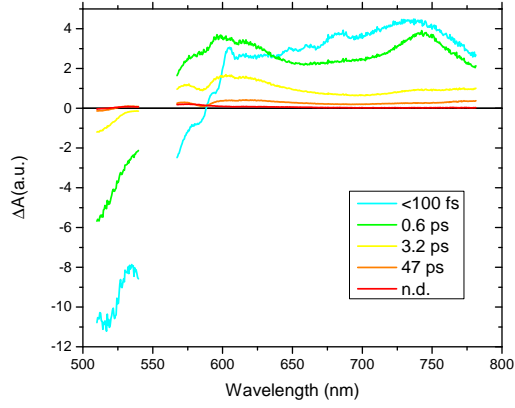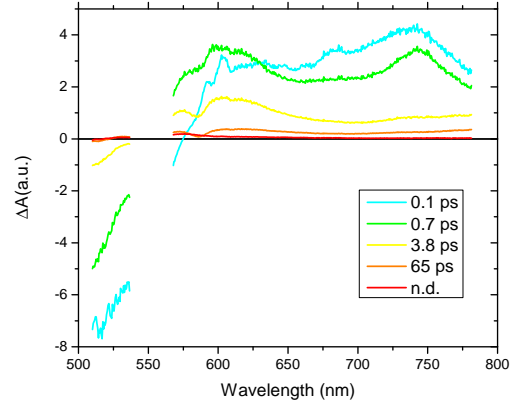
(b) BX4
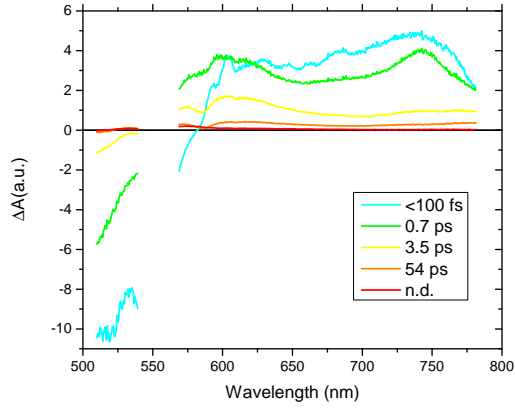
(c) BU1

(d) BY23

Figure 5.3: EADS in a VIS region resulting from the global fitting analysis.

which no Car signal is observed. The fifth EADS (red) does not contain any signal, it is so-called non-decaying component. Therefore, the orange EADS decaying in 47 ps has to correspond to the successful energy trapping in RC.

	X1	BX4	BU1	BY23
τ_1	<100 fs*	0.1 ps*	<100 fs*	<100 fs*
τ_2	0.6 ps	0.7 ps	0.7 ps	0.6 ps
τ_3	3.2 ps	3.8* ps	3.5 ps	3.3 ps
τ_4	47 ps	65 ps	54 ps*	40 ps

Table 5.1: Time constants obtained by global fitting analysis for measurements in the VIS region. The symbol * represents fixed time constants.

In comparison with global fitting results of another samples in Fig. 5.3, it can be concluded that no significant differences are observed, besides the lower intensity of the ICT state in the case of BY23 mutant. Even time constants obtained by global fitting are more or less the same, for better clarity being compared in Table 5.1.

To get an insight into the Car $\rightarrow$ Bchl energy transfer dynamics, the NIR region where Bchl Q_y bleaching is observed has been probed. Transient absorption spectra with the strongest Bchl Q_y bleaching, i.e. those at 1.7 ps, were then extracted and they are all shown in Fig. 5.4.
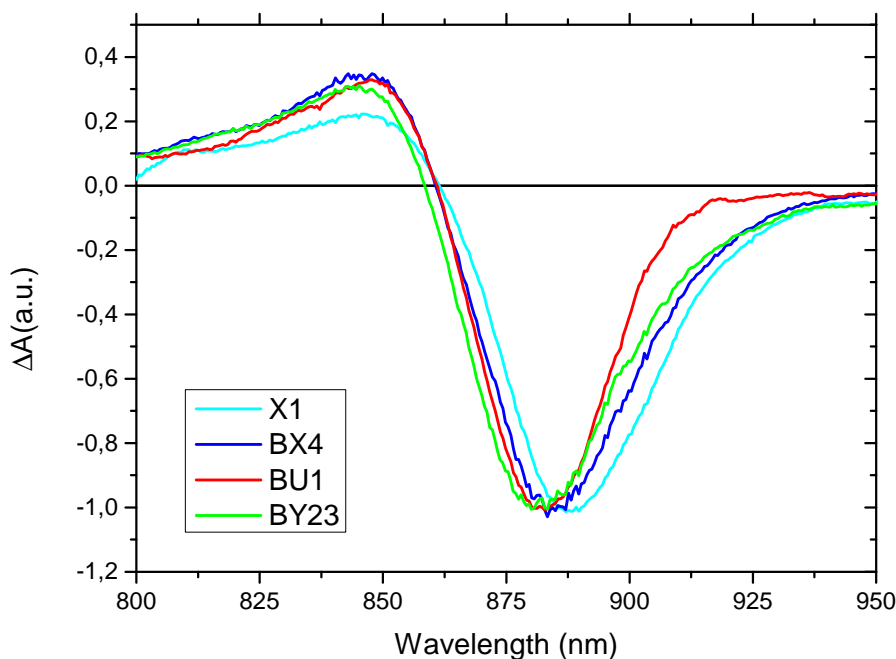

Figure 5.4: Transient absorption spectra of all measured mutants in the NIR region after 555 nm excitation, taken at 1.7 ps and normalized to the maximum of Bchl Q_y bleaching.

The profound Bchl Q_y bleaching signal in the NIR region demonstrates the fact that the energy is transferred from Car(s) to Bchl(s). By comparing the shape of such signal in Fig. 5.4 for particular mutants, it can be concluded that the Q_y bleaching seems more or less similar in all measured samples. There are, however, few exceptions which are worth mentioning: a redder part of BU1 Q_y bleaching is narrower in comparison with the rest of samples and even positions of Q_y bleaching maximum vary within the mutants. The different positions of Q_y bleaching maximum might seem surprising because the BY23 mutant is the only one with shifted Q_y maximum in steady-state

absorption spectra (see Fig. 5.1). Therefore, it is the only sample in which one would expect a shift of Q_y bleaching.

The results of global fitting analysis of NIR data in the form of EADS will be also presented (see Fig. 5.5).
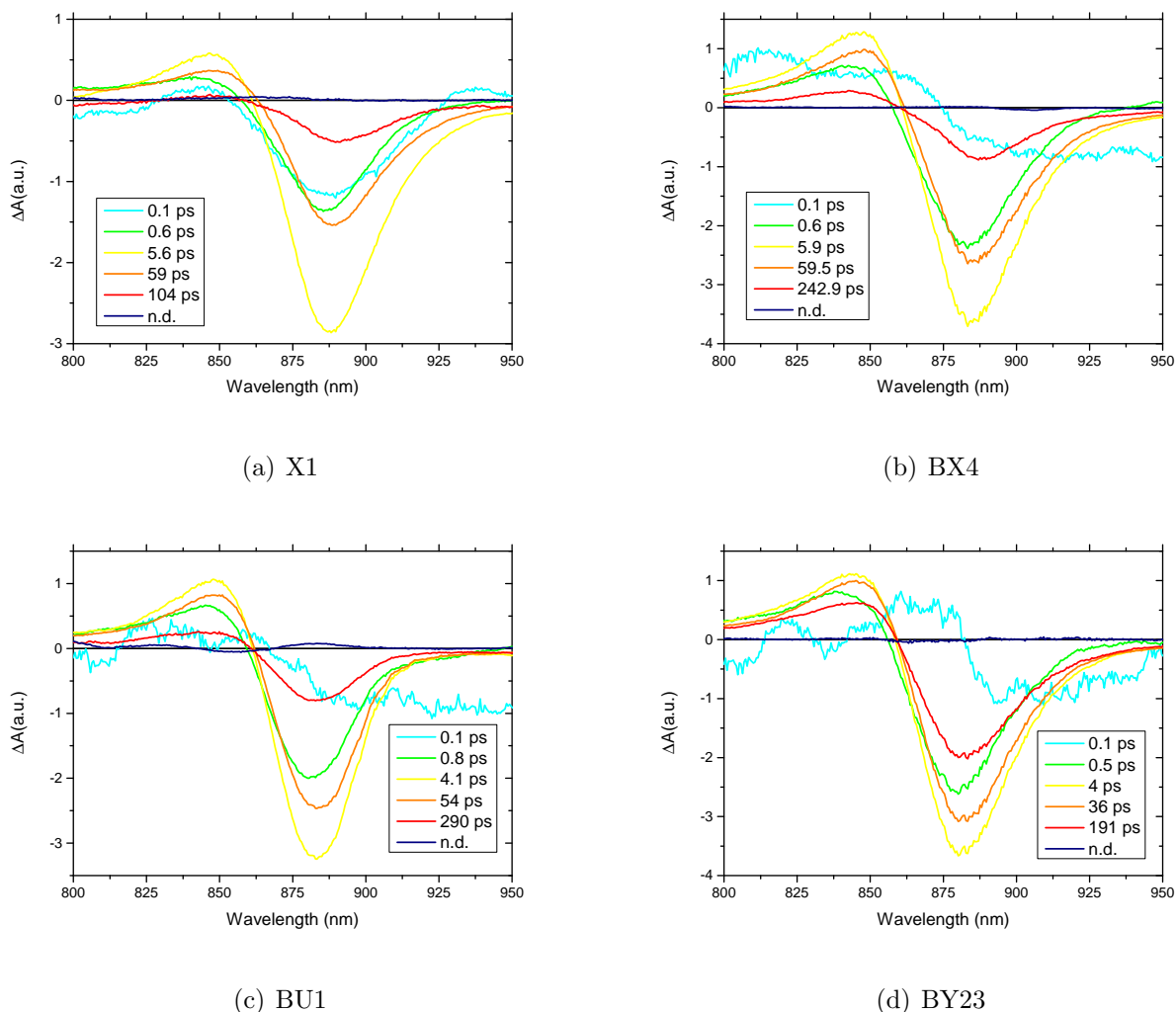

(a) X1

(b) BX4

(c) BU1

(d) BY23

Figure 5.5: EADS in a NIR region resulting from the global fitting analysis.

Similarly to previous EADS in the VIS region, only X1 mutant will be described in more detail as no significant differences are observed among the measured mutants. The first EADS (cyan) decays in 0.1 ps and it already contains a hint of Bchl bleaching signal which is related to the energy transfer from Car(s). At the same time, the second EADS appears, later decaying in 0.6 ps. The similar time constant also occurrs in the VIS EADS (see Fig. 5.3), therefore, it supports the S_1/ICT energy transfer. The third EADS (yellow) decaying at 5.6 ps possesses the largest Bchl Q_y bleaching signal. This EADS also has the corresponding component in the VIS data and as has been mentioned above, the possible events will be discussed. The fourth EADS (orange) corresponding to

	X1	BX4	BU1	BY23
τ_1	0.1 ps*	0.1 ps*	0.1 ps*	0.1 ps*
τ_2	0.6 ps	0.7 ps	0.7 ps	0.5 ps
τ_3	5.6 ps	5.9 ps	4.1 ps*	4 ps
τ_4	60 ps	59 ps*	57 ps	36 ps
τ_5	104 ps	242 ps	290 ps	191 ps

Table 5.2: Time constants obtained by global fitting analysis for measurements in the NIR region. The symbol * represents fixed time constants.

the Bchl $\rightarrow$ RC energy transfer decays in 59 ps, giving rise to another component (red) decaying in 104 ps. At this time, a majority of Bchl Q_y bleaching signal has dissapeared. The origin of the last time constant is questionable. It can indicate the presence of LH1 complexes without the RC. Furthermore, this time constant could also appear due to the closed reaction centers. [60] Both mentioned events could cause a longer decay of Bchls. Again, all time constants obtained by global fitting analysis of the measurements in the NIR region are compared in Table 5.2.

5.3 Kinetics

Next, kinetics corresponding to appropriate excited states will be presented as they can reveal some changes in excited-state dynamics. Potential disruption of spheroidenone s-*trans* configuration has already been suggested based on the transient absorption spectra in Fig. 5.2 where a decrease of the ICT state intensity for the BY23 mutant can be observed. Besides the lower intensity of the ICT state, the s-*trans* disruption can also affect the rate of spheroidenone excited-state decays. Thus, kinetics of the S_1 and ICT state were extracted and they are shown in Fig. 5.6 and Fig 5.7, respectively.

By comparing the kinetics of the S_1 state in Fig. 5.6, it can be concluded that X1, BX4 and BU1 mutant S_1 kinetics are identical. On the other hand, the BY23 decay is slightly slower. It may seem strange that no difference is observed in the S_1 state appearance in Fig. 5.2 but one has to take into account that all presented transient absorption spectra are normalized at the region of the S_1 state. Therefore, no information about the S_1 state appearance can be obtained from such comparison.
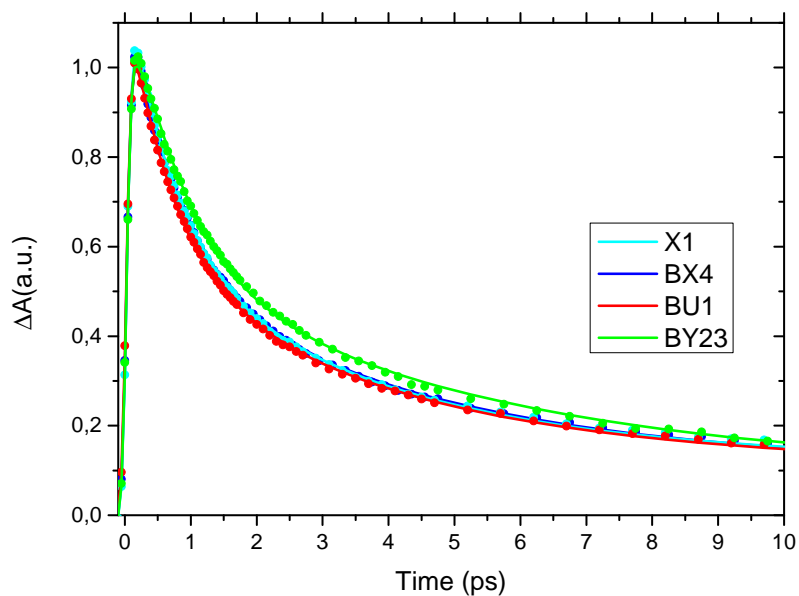
Figure 5.6: Kinetics showing the decaying of the S1 state for all measured samples. Kinetics were taken at 615 nm and normalized to the maximum of their corresponding fits.
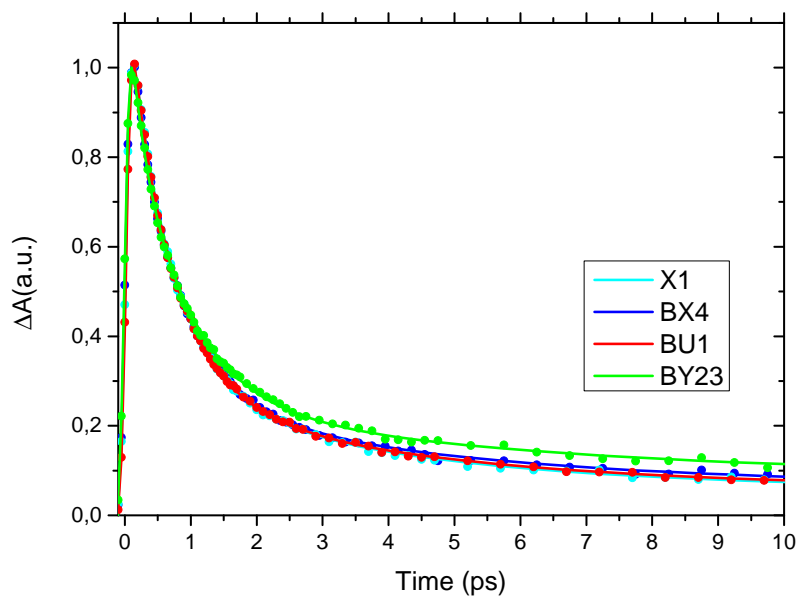

Figure 5.7: Kinetics showing the decaying of the ICT state for all measured samples. Kinetics were taken at 742 nm and normalized to the maximum of their corresponding fits.

By taking a look at the kinetics of the ICT state in Fig 5.7, similar trend as in the case of the S_1 state is observed; X1, BX4 and BU1 mutants are identical and BY23 mutant more or less matches the rest of samples. At later times, it slightly deviates. Thus, both the discussed kinetics indicate that the behavior of BY23 mutant differs from the rest of mutants but only to a limited extent.

To be consistent, kinetics of Bchl Q_y bleaching should also be presented. They are all shown in Fig. 5.8. By comparing them, it can be concluded that the kinetics differ one from the other, except for BX4 and BU1 mutants whose kinetics are identical again. It is worth mentioning that the Bchl Q_y bleaching of BY23 mutant decays the slowest.
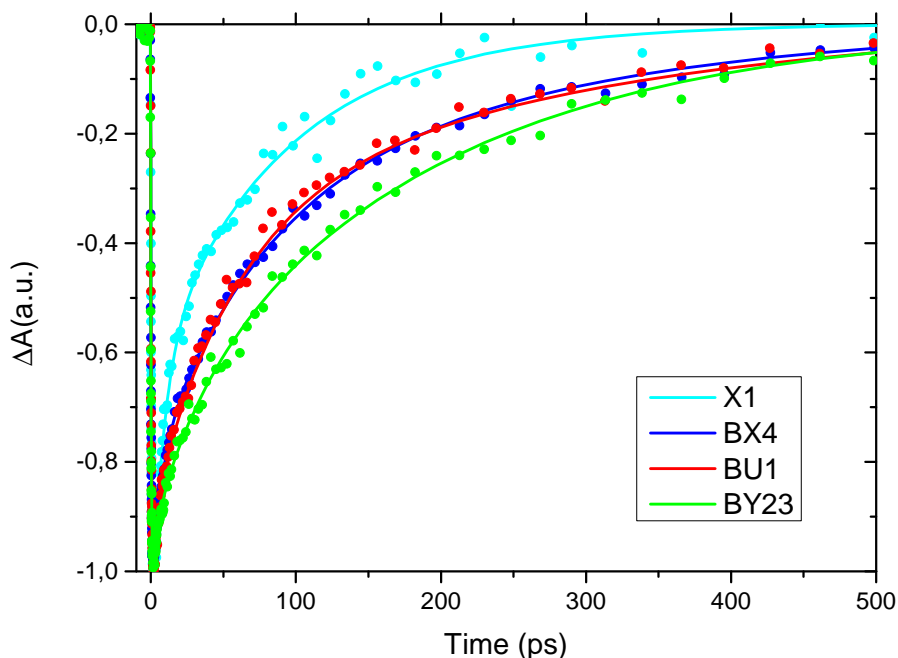

Figure 5.8: Kinetics showing the decaying of the Bchl Q_y bleaching for all measured samples. Kinetics were taken at the maximum of the Bchl Q_y bleaching of particular mutants (see Fig. 5.4) and normalized to the minimum of their corresponding fits.

6 Discussion

Despite the huge variety of light-harvesting complexes in nature, a unique behavior of the RC-LH1 spn PufX complex makes this particular photosynthetic unit the object of our interest. An incorporation of the CC spheroidenone into the structure of the RC-LH1 spn PufX complex results not only in the appearance of the ICT state but also in the activation of the additional S_1/ICT energy transfer pathway. [1] Furthermore, such results suggest the existence of a specific spheroidenone binding interaction. This specific interaction likely forces the carotenoid to adopt the s-*trans* configuration, which is considered a crucial condition for the ICT state activation in spheroidenone. Based on the hypothesis described in section 3.5.2, Trp and Tyr residues at the end of N-terminal domains of LH1 α and β polypeptides were replaced by Phe to hinder the potentially existing hydrogen bond interaction between the AA and the carotenoid keto group. Transient absorption spectra in Fig. 5.2 indicate that the AA substitution of BY23 mutant (αTrp-24 $\rightarrow$ Phe) causes a decrease of the ICT signal. However, it cannot be ultimately claimed that αTrp-24 is the ICT state activator we were looking for due to following reasons. First, such large structural change as the s-*trans* $\rightarrow$ s-*cis* transformation would definitely affect the spheroidenone excited-state dynamics. By comparing Figs. 5.6 and 5.7, it can be concluded that the behavior of BY23 mutant only slightly differs from the rest of mutants. Secondly, time constants resulting from the global fitting analysis in the VIS region (see Table 5.1) are more or less the same. This supports the idea that the excited-state dynamics of spheroidenone remains preserved in all measured mutants. On the other hand, data obtained from the measurements in the NIR region revealed that Bchl dynamics might be affected more as the differences between the transient absorption spectra (see Fig. 5.4) and even kinetics (see Fig. 5.8) seem to be more significant.

The role of the αTrp-24 residuum

Results described in Chpt. 5 indirectly indicate that αTrp-24 $\rightarrow$ Phe mutation affects a behavior of the whole RC-LH1 spn PufX unit. It is worth mentioning that αTrp-24 is a part of the highly conserved so-called KIW (Lys-Ile-Trp) motif which was examined in detail due to its potential influence on the RC-LH1 complex structure and functions. Therefore, it has already been described that αTrp-24 plays a role in spheroidenone binding in the LH1 complex of *Rba. capsulatus*. αTrp-24 $\rightarrow$ Tyr mutation results in a decrease of bound carotenoids. [61] On the other hand, a duplication of the whole KIW motif causes an increase of carotenoids bound to the LH1 unit. [62] Quite recently, even the α subunit of *Rba. sphaeroides* LH1 complex with αTrp-24 $\rightarrow$ Phe mutation was examined and a decreased number of bound carotenoids has also been confirmed. [63] It means that our mutant BY23 must possess the same feature. To support this hypothesis, the HPLC analysis of all measured mutants has been performed and a decreased number of Cars bound to the LH1 complex of BY23 mutant was confirmed. By comparing the structure of Trp, Tyr and Phe AAs, it can be said that they are all very similar. Therefore, it might seem quite surprising that the αTrp-24 mutation to either Tyr or Phe has such a significant effect on the number of bound carotenoids in LH1 complex. One of the possible explanations could be a slightly larger structure of Trp. [62] To conclude, αTrp-24 $\rightarrow$ Phe mutation likely caused a decreased number of spheroidenone molecules bound to the LH1 complex.

Spheroidenone binding is not the only function of αTrp-24 residuum. It has been discovered that αTrp-24 also affects the assembly of the whole RC-LH1 complex and its substitution to Ala or Leu can result in the presence of RCs without the surrounding LH1 ring. [61] By taking a closer look at the steady-state absorption spectra in Fig. 5.1, it can be noticed that maxima of BY23 RC pigment bands are higher than those of other mutants, even after normalization. Furthermore, the HPLC analysis has confirmed that the Bchl/BPheo ratio of BY23 mutant is lower than Bchl/BPheo ratios of other mutants. Bacteriopheophytins are the pigments of RC. Therefore, based on the HPLC results, there might be some free RCs in our BY23 sample.

Spheroidenone binding sites: complexity vs. specificity

In LH1 complex of *Rba. sphaeroides*, however, there are two spheroidenone molecules bound to one $\alpha\beta$ subunit. [48] Unfortunately, due to the fact that exact spheroidenone binding sites in the LH1 complex of *Rba. sphaeroides* are unknown, it is difficult to determine how the αTrp-24 $\rightarrow$ Phe mutation could affect the binding of one or even both spheroidenones. Nevertheless, our results suggest the following hypothesis about the specificity of spheroidenone binding sites. The first spn binding site preserves the s-*trans* configuration of the spheroidenone. As a result, the high intensity of the ICT state is observed. On the other hand, the spheroidenone bound at the second binding site need not be necessarily maintained at the exact s-*trans* configuration. Therefore, the contribution of the non-s-*trans* spheroidenone to the ICT state intensity would be less significant. To conclude, spheroidenones binding sites in LH1 complex appear to be more complex and the stabilisation of whichever spheroidenone configuration does not probably take place only due to the single interaction. The αTrp-24 $\rightarrow$ Phe mutation could then lower the number of the s-*trans* spheroidenones bound to the LH1 complex. This fact could explain a decreased ICT intensity of BY23 mutant observed in its transient absorption spectrum (Fig. 5.2).

Based on the EADS spectra, another support of our hypothesis arises. The hypothesis about spheroidenone binding site specificity could also explain the origin of the $\sim$3.5 ps time constant in the VIS EADS spectra (see Fig. 5.3 and Table 5.1) as the decaying time constant of the non-s-*trans* spheroidenone, which is characterized by a lower ICT state signal. Because there is no increase of the bleaching in the NIR region associated with this time constant, the non-s-trans spheroidenone does not transfer energy to BChl. A support for this suggestion comes from the similarity of the decay time of 3.5 ps of the complex and the 6 ps lifetime of spheroidenone in solution. [2] Spheroidenone in solution presumably adopts the s-*cis* configuration meaning that the number of conjugated bonds is $N=10$ and the carbonyl group is not part of the conjugation. The difference between the respective numbers can be ascribed to an interference with parallel processes in the complex system or to a partial involvement of the carbonyl group into the conjugation.

Nevertheless, the NIR EADS also possess a similar $\sim$5 ps time constant (Table 5.2), attributed to Bchl dynamics. We suggest two following explanations for the relationship

between the similar time constants in VIS and in NIR regions. First, there are two different events in the VIS and NIR region which have a similar time constant by coincidence. Secondly, the ∼5 ps component of the NIR region could also appear in the VIS region. Thus, the ∼3.5 ps time constant would be associated with Bchl dynamics and not with the decay of the non-s-trans spheroidenone as discussed above.

Another important fact about the already-mentioned KIW motif that fits into this section is that it is also present in LH2 complexes. [64] However, LH2 spn complex does not exhibit any ICT related signal. [1] Therefore, the carotenoid binding site in LH2 may possess some specific interactions which would disable the stabilisation of the spheroidenone s-*trans* configuration. Yet, for now, such interactions have not been found. [64] Consequently, it disproves the assumption that αTrp-24 is the ICT state activator.

The effect of AA mutations on bacteriochlorophylls

As has been mentioned in the first paragraph of this section, our AA mutations might have some effects on Bchl molecules. First hint of such effects can be seen in steady-state absorption spectra in Fig. 5.1 as the Bchl Q_y maximum of BY23 mutant is obviously shifted to 872 nm with respect to the rest of mutants possessing the Q_y maximum at ∼875 nm. Furthermore, this idea is also supported by differences recorded in Bchl transient absorption spectra (Fig. 5.4) and kinetics (Fig. 5.8). However, the differences in Bchl dynamics are observed even for BX4 and BU1 mutants whose behavior is almost identical as that of X1 mutant in the case of Car excited-state dynamics. This may mean that αTyr-27 → Phe, βTyr-30 → Phe and αTrp-24 → Phe mutations could probably have similar effect on Bchls. This hypothesis is also supported by their similar positions within the $\alpha\beta$ subunit. By comparing the Bchl Q_y bleaching kinetics, it can be noticed that BY23 mutant (αTrp-24 → Phe) affects the Bchl decaying more than BX4 and BU1 mutants. However, it can be explained by overall effects of the αTrp-24 → Phe mutation on the arrangement of RC-LH1 complex that have been discussed above.

Considering the positions of αTyr-27, βTyr-30 and αTrp-24 with respect to Bchls which are located near the C-terminal domains of α and β polypeptides (i.e. on the opposite end of the $\alpha\beta$ subunit), the potential effects on Bchls would have to be very indirect and long-range. One can suppose the existence of various mutual interactions between all three mentioned AA residues which would be partly disrupted by the Phe

mutations. These interactions could help to stabilise the positions of α and β N-terminal domains, i.e. to stabilise the overall shape of the $\alpha\beta$ subunit. Such structural deviations could indirectly affect the already confirmed Bchl $\leftrightarrow$ Trp residues interactions. For instance, the interaction of Bchl with αTrp43 which is located near the C-terminus. [65]

To conclude, what could be the actual origin of the ICT state activation in LH1 complex of *Rba. sphaeroides*? Based on the results obtained by time-resolved experiments, the stabilisation of a spheroidenone keto group is likely not due to the single hydrogen bond interaction with the closest AA residue but the whole functional group is probably somehow stabilised to the s-*trans* configuration by various interactions. The same (or at least similar) mechanism of carotenoid binding and related s-*trans* Car stabilisation can also be valid for other organisms possessing CCs in their LH1 complexes. For instance, the spheroidenone bound in RC-LH1 complex of *Roseobacter sp.* COL2P [66] or the diketospirilloxanthin bound in RC-LH1 complex of *Rba. sphaeroides.* [56] For the purpose of potential future experiments, we suggest the substitution of two AAs in one mutant to avoid a potential compensation of a missing interaction.

7 Conclusion

The main task of this thesis was to perform time-resolved pump-probe experiments of mutated RC-LH1 PufX spn complexes of *Rb. sphaeroides*. The second task of such measurements was to find out if one of the AA substitutions is able to switch off the ICT state observed in non-mutated RC-LH1 PufX spn complexes. The experiments in the VIS region revealed that there are not any significant differences at the Car excited-state dynamics. Despite the fact that a decreased intensity of the ICT state was observed for BY23 mutant with αTrp-24 $\rightarrow$ Phe mutation, we suppose that αTrp-24 is not the ICT state activator due to various reasons discussed above.

Based on the obtained results, we suggest the hypothesis about the specificity of carotenoid binding sites within the $\alpha\beta$ subunit. The first carotenoid adopts the s-*trans* configuration, therefore, it exhibits the ICT signal. The second carotenoid does not possess the exact s-*trans* configuration and its contribution to the ICT state intensity is lower than the contribution of the former Car. Moreover, our results support the idea that the αTrp-24 $\rightarrow$ Phe mutation causes a decreased number of the s-*trans* spheroidenones bound to the LH1 complex, through which the decreased ICT signal of BY23 mutant can be explained.

As a result, we may thus conclude that the stabilisation of the spn s-*trans* configuration is probably a more complex process involving more AA residues or even the carotenoid binding site as a whole. Quite surprisingly, more significant differences have been observed for the Bchl dynamics in the NIR region. Thereby we conclude that Bchls might be more sensitive to the primary structure of $\alpha\beta$ protein subunit.

Bibliography

[1] Šlouf V, Chábera P, Olsen JD, Martin EC, Qian P, Hunter CN, Polívka T (2012) *Photoprotection in a purple phototrophic bacterium mediated by oxygen-dependent alteration of carotenoid excited-state properties* Proc Natl Acad Sci USA, 109:8570-8575

[2] Zigmantas D, Hiller RG, Sharples FP, Frank HA, Sundstrom V, Polívka T (2004) *Effect of a conjugated carbonyl group on the photophysical properties of carotenoids* Phys Chem Chem Phys, 6:3009-3016

[3] Šlouf V (2013) *Protein control over carotenoid spectroscopy and functions* Ph.D. Thesis, University of South Bohemia, Faculty of Science, České Budějovice, CZ

[4] Kodíček M, Karpenko V (2013) *Biofyzikální chemie* Academia, Praha, CZ

[5] Atkins P, Friedman R (2011) *Molecular Quantum Mechanics* Oxford University Press, Oxford, UK

[6] Gilbert A, Baggott J (1991) *Essentials of Molecular Photochemistry* CRC Press, London, UK

[7] Hollas MJ (2004) *Modern Spectroscopy* John Wiley & Sons Ltd, Chicester, UK

[8] Green BR, Parson WW (2003) *Light-Harvesting Antennas in Photosynthesis* Kluwer Academic Publishers, Dordrecht, NE

[9] Walla PJ (2009) *Modern Biophysical Chemistry* WILEY-VCH Verlag GmbH & Co. KGaA, Weinheim, DE

[10] Blankenship RE (2002) *Molecular Mechanisms of Photosynthesis* Blackwell Science Ltd, Oxford, UK

[11] Dexter DL (1953) *A Theory of Sensitized Luminescence in Solids* J Chem Phys, 21: 836-850

[12] Frank HA, Young A, Britton G, Cogdell RJ (1999) *The Photochemistry of Carotenoids* Springer Netherlands, Dordrecht, NE

[13] Polívka T, Frank HA (2010) *Molecular Factors Controlling Photosynthetic Light Harvesting by Carotenoids* Acc Chem Res, 43(8):1125–1134

[14] Britton G, Liaaen-Jensen S, Pfander H (2008) *Carotenoids, Volume 4: Natural Functions* Birkhäuser Verlag, Basel, CH

[15] Polívka T, Sundström V (2004) *Ultrafast Dynamics of Carotenoid Excited States — From Solution to Natural and Artificial Systems* Chem Rev, 104(4):2021-2071

[16] Šlouf V (2009) *Energy transfer pathways in the intrinsic light harvesting complex of Amphidinium carterae* Mgr. Thesis, University of South Bohemia, Faculty of Science, České Budějovice, CZ

[17] Wehling A, Walla PJ (2005) *Time-Resolved Two-Photon Spectroscopy of Photosystem I Determines Hidden Carotenoid Dark-State Dynamics* J Phys Chem B, 109(51):24510–24516

[18] Fiedor L, Heriyanto, Fiedor J, Pilch M (2016) *Effects of Molecular Symmetry on the Electronic Transitions in Carotenoids* J Phys Chem Lett, 7(10):1821–1829

[19] Frank HA, Desamero RZB, Chynwat V, Gebhard R, van der Hoef I, Jansen FJ, Lugtenburg J, Gosztola D, Wasielewski MR (1997) *Spectroscopic Properties of Sheproidene Analogs Having Different Extents of π Electron Conjugation* J Phys Chem A, 101:149-157

[20] DeCoster B, Christensen RL, Gebhard R, Lugtenburg J, Farhoosh R, Frank HA (1992) *Low-lying Electronic States of Carotenoids* Biochim Biophys Acta, 1102(1):107-14

[21] Bautista JA, Connors RE, Raju BB, Hiller RG, Sharples FP, Gosztola D, Wasielewski MR, Frank HA (1999) *Excited State Properties of Peridinin: Observation of a Solvent Dependence of the Lowest Excited Singlet State*

Lifetime and Spectral Behavior Unique among Carotenoids J Phys Chem B, 103(41):8751–8758

[22] Kopczynski M, Ehlers F, Lenzer T, Oum K (2007) *Evidence for an Intramolecular Charge Transfer State in 12-Apo-β-caroten-12-al and 8-Apo-β-caroten-al: Influence of Solvent Polarity and Temperature* J Phys Chem A, 111(25):5370-5381

[23] Kosumi D, Fujii R, Sugisaki M, Oka N, Iha M, Hashimoto H (2014) *Characterization of the Intramolecular Transfer State of Marine Carotenoid Fucoxanthin by Femtosecond Pump-probe Spectroscopy* Photosynth Res, 121:61–68

[24] Polívka T, Kaligotla S, Chábera P, Frank HA (2011) *An Intramolecular Charge Transfer State of Carbonyl Carotenoids: Implications for Excited State Dynamics of Apo-carotenals and Retinal* Phys Chem Chem Phys, 22(13):10787-10796

[25] Zigmantas D, Polívka T, Hiller RG, Yartsev A, Sundström V (2001) *Spectroscopic and Dynamic Properties of the Peridinin Lowest Singlet Excited States* J Phys Chem A, 105(45):10296-10306

[26] West RG, Fuciman M, Staleva-Musto H, Šebelík V, Bína D, Durchan M, Kuznetsova V, Polívka T (2018) *Equilibrium Dynamics of S1 and ICT States of Fucoxanthin in Solution as revealed by Multi-Pulse Spectroscopy: Dependence on Polarity, Proticity, and Temperature* J Phys Chem B, 122(29):7264-7276

[27] Ilagan RP, Christensen RL, Chapp TW, Gibson GN, Pascher T, Polívka T, Frank HA (2005) *Femtosecond Time-resolved Absorption Spectroscopy of Astaxanthin in Solution and in α-Crustacyanin* J Phys Chem A, 109(14):3120-3127

[28] Kopczynski M, Lenzer T, Oum K, Seehusen J, Seidela MT, Ushakova VG (2005) *Ultrafast Transient Lens Spectroscopy of Various C40 Carotenoids: Lycopene, Beta-carotene, (3R,3'R)-zeaxanthin, (3R,3'R,6'R)-lutein, Echinenone, Canthaxanthin, and Astaxanthin* Phys Chem Chem Phys, 14(7):2793-2803

[29] Chábera P, Fuciman M, Hříbek P, Polívka T (2009) *Effect of Carotenoid Structure on Excited-state Dynamics of Carbonyl Carotenoids* Phys Chem Chem Phys, 39(11):8795–8803

[30] Takaichi S, Furihata K, Harashima K (1991) *Light-induced changes of carotenoid pigments in anaerobic cells of the aerobic photosynthetic bacterium, Roseobacter*

denitrificans (Erythrobacter species OCh 114): reduction of spheroidenone to 3,4-dihydrospheroidenone Arch Microbiol, 155:473-476

[31] Vaswani HM, Holt NE, Fleming GE (2005) *Carotenoid–chlorophyll complexes: Ready-to-harvest* Pure Appl Chem, 77(6):925–945

[32] Macpherson AN, Arellano JB, Fraser NJ, Cogdell RJ, Gillbro T (2001) *Efficient Energy Transfer from the Carotenoid S2 State in a Photosynthetic Light-Harvesting Complex* Biophys J, 80(2):923-930

[33] Walla PJ, Linden PA, Hsu CP, Scholes GD, Fleming GR (2000) *Femtosecond dynamics of the forbidden carotenoid S-1 state in light-harvesting complexes of purple bacteria observed after two-photon excitation* Proc Natl Acad Sci USA, 97(20):10808-10813

[34] Kosumi D, Nishiguchi T, Amao Y, Cogdell RJ, Hashimoto H (2018) *Singlet and triplet excited states dynamics of photosynthetic pigment chlorophyll a investigated by sub-nanosecond pump-probe spectroscopy* J Photochem Photobiol A, 358:374-378

[35] Damjanović A, Ritz T, Schulten K (1999) *Energy transfer between carotenoids and bacteriochlorophylls in light-harvesting complex II of purple bacteria* Phys Rev E, 59(3):3293-3311

[36] Frahmcke JS, Walla PJ (2006) *Coulombic couplings between pigments in the major light-harvesting complex LHC II calculated by the transition density cube method* Chem Phys Lett 430:397–403

[37] Krueger BP, Scholes GD, Fleming GR (1998) *Calculation of Couplings and Energy-Transfer Pathways between the Pigments of LH2 by the ab Initio Transition Density Cube Method* J Phys Chem B, 102(27):5378–5386

[38] Vinklarek IS, Bornemann TLV, Lokstein H, Hofmann E, Alster J, Pšenčík J (2018) *Temperature Dependence of Chlorophyll Triplet Quenching in Two Photosynthetic Light-Harvesting Complexes from Higher Plants and Dinoflagellates* J Phys Chem B, 122(38):8834-8845

[39] Kvíčalová Z, Alster J, Hofmann E, Khoroshyy P, Litvín R, Bína D, Polívka T, Pšenčík J (2016) *Triplet-triplet energy transfer from chlorophylls to carotenoids in*

two antenna complexes from dinoflagellate Amphidinium carterae Biochim Biophys Acta, Bioenerg, 1857(4):341-349

[40] Müller P, Li XP, Niyogi KK (2001) *Non-Photochemical Quenching: A Response to Excess Light Energy* Plant Physiol, 125:1559-1566

[41] McDermott G, Prince GM, Freer AA, Hawthornthwaite-Lawless AM, Papiz MZ, Cogdell RJ, Isaacs NW (1995) *Crystal structure of an integral membrane light-harvesting complex from photosynthetic bacteria* Nature, 374:517–521

[42] Arellano JB, Rajut BB, Naqvi KR, Gillbro T (1998) *Estimation of Pigment Stoichiometries in Photosynthetic Systems of Purple Bacteria: Special Reference to the (Absence of) Second Carotenoid in LH2* Photochem Photobiol, 68(1):84-87

[43] van Mourik F, Hawthornthwaite AM, Vonk C, Evans MB, Cogdell RJ, Sundström V, Grondelle R (1992) *Spectroscopic characterization of the low-light B800-850 light-harvesting complex of Rhodopseudomonas palustris, strain 2.1.6* Biochim Biophys Acta, Bioenerg, 1140(1):85-93

[44] Hu X, Ritz T, Damjanović A, Autenrieth F, Schulten K (2002) *Photosynthetic apparatus of purple bacteria* Q Rev Biophys, 35(1):1–62

[45] Picorel R, Belanger G, Gingras G (1983) *Antenna holochrome B880 of Rhodospirillum rubrum S1. Pigment, phospholipid, and polypeptide composition* Biochemistry, 22(10):2491–2497

[46] Cogdell RJ, Lindsay JG, Valentine J, Durant I (1982) *A further characterisation of the B890 light-harvesting pigment-protein complex from Rhodospirillum rubrum strain S1* FEBS Lett, 150(1):151-154

[47] Broglie RM, Hunter CN, Delepelaire P, Niederman RA, Chua NH, Clayton RK (1980) *Isolation and characterization of the pigment-protein complexes of Rhodopseudomonas sphaeroides by lithium dodecyl sulfate/polyacrylamide gel electrophoresis* Proc Natl Acad Sci USA, 77(1):87-91

[48] Woronowicz K, Olubanjo OB, Sung HC, Lamptey JL, Niederman RA (2011) *Differential assembly of polypeptides of the light-harvesting 2 complex encoded by distinct operons during acclimation of Rhodobacter sphaeroides to low light intensity* Photosynth Res, 111:125–138

[49] Picorel R, Lu T, Holt RE, Cotton TM, Seibert M (1990) *Surface-enhanced resonance Raman scattering spectroscopy of bacterial photosynthetic membranes: orientation of the carotenoids of Rhodobacter sphaeroides 2.4.1* Biochemistry, 29:707-712

[50] Šlouf V, Kuznetsova V, Fuciman M, Carbon CB, Wilson A, Kirilovsky D, Polívka T (2017) *Ultrafast spectroscopy tracks carotenoid configurations in the orange and red carotenoid proteins from cyanobacteria* Photosynth Res, 131:105–117

[51] Wilson A, Kinney JN, Zwart PH, Punginelli C, D'Haene S, Perreau F, Klein M, Kirilovsky D, Kerfeld CA (2010) *Structural Determinants Underlying Photoprotection in the Photoactive Orange Carotenoid Protein of Cyanobacteria* J Biol Chem, 285(24):18364 –18375

[52] Bandara S, Ren Z, Lu L, Zeng X, Shin H, Zhao KH, Yang X (2017) *Photoactivation mechanism of a carotenoid-based photoreceptor* Proc Natl Acad Sci 114:6286-6291

[53] Swainsbury DJK, Faries KM, Niedzwiedski DM, Martin EC, Flinders AJ, Canniffe DP, Shen G, Bryant DA, Kirmaier CH, Holten D, Hunter CN (2018) *Engineering of B800 bacteriochlorophyll binding site specificity in the Rhodobacter sphaeroides LH2 antenna* Biochim Biophys Acta, Bioenerg, 860(3):209-223

[54] Zeng X, Choudhary M, Kaplan S (2003) *A Second and Unusual pucBA Operon of Rhodobacter sphaeroides 2.4.1: Genetics and Function of the Encoded Polypeptides* J Bacteriol, 185:6171-6184

[55] Pugh RJ, McGlynn P, Jones MR, Hunter CN (1998) *The LH1-RC core complex of Rhodobacter sphaeroides: interaction between components, time-dependent assembly, and topology of the PufX protein* Biochim Biophys Acta - Bioenergetics, 1336:301-316

[56] Šlouf V, Keşan G, Litvín R, Swainsbury DJK, Martin EC, Hunter CN, Polívka T (2017) *Carotenoid to bacteriochlorophyll energy transfer in the RC-LH1-PufX complex from Rhodobacter sphaeroides containing the extended conjugation keto-carotenoid diketospirilloxanthin* Photosynth Res, 135:33-43

[57] Berera R, van Grondelle E, Kennis JTM (2009) *Ultrafast transient absorption spectroscopy: principles and application to photosynthetic system* Photosynth Res, 101:105–118

[58] Keşan G, Litvín R, Bína D, Durchan M, Šlouf V, Polívka T (2016) *Efficient light-harvesting using non-carbonyl carotenoids: Energy transfer dynamics in the VCP complex from Nannochloropsis oceanica* Biochim Biophys Acta, Bioenerg, 1857(4):370-379

[59] West RG (2018) *Carotenoid Excited State Processes by Femtosecond Time-Resolved Pump-Probe and Multi-Pulse Spectroscopies* Ph.D. Thesis, University of South Bohemia, Faculty of Science, České Budějovice, CZ

[60] Hess S, Visscher K, Ulander J, Pullerits T, Jones MR, Hunter CN, Sundström V (1993) *Direct Energy Transfer from the Peripheral LH2 Antenna to the Reaction Center in a Mutant of Rhodobacter sphaeroides That Lacks the Core LH1 Antenna* Biochemistry, 32:10314-10322

[61] Babst M, Albrecht H, Wegmann I, Brunisholz R, H Zuber (1991) *Single amino acid substitutions in the B870 α and β light-harvesting polypeptides of Rhodobacter capsulatus* Eur J Biochem, 202:277-284

[62] Richter P, Brand M, Drews G (1992) *Characterization of LHI- and LHI+ Rhodobacter capsulatus pufA mutants* J Bacteriol, 174(9):3030-3041

[63] Olsen JD, Martin EC, Hunter CN (2017) *The PufX quinone channel enables the light-harvesting 1 antenna to bind more carotenoids for light collection and photoprotection* FEBS Lett 591:573–580

[64] Niedzwiedzki DM, Dilbeck PL, Tang Q, Martin EC, Bocian DF, Hunter CN, Holten D (2016) *New insights into the photochemistry of carotenoid spheroidenone in light-harvesting complex 2 from the purple bacterium Rhodobacter sphaeroides* Photosynth Res, 131:291–304

[65] Olsen JD, Sockalingum GD, Robert B, Hunter CN (1994) *Modification of a hydrogen bond to a bacteriochlorophyll a molecule in the light-harvesting 1 antenna of Rhodobacter sphaeroides* Proc Nat Acad Sci USA, 91:7124-7128

[66] Šlouf V, Fuciman M, Dulebo A, Kaftan D, Koblížek M, Frank HA, Polívka T (2013) *Carotenoid Charge Transfer States and Their Role in Energy Transfer Processes in LH1–RC Complexes from Aerobic Anoxygenic Phototrophs* J Phys Chem B, 117(38):10987–10999